

Melanopsin-dependent photo-perturbation reveals desynchronization underlying the singularity of mammalian circadian clocks

Hideki Ukai^{1,10}, Tetsuya J. Kobayashi^{1,4,10}, Mamoru Nagano⁵, Koh-hei Masumoto¹, Mitsugu Sujino⁵, Takao Kondo⁶, Kazuhiro Yagita^{7,8}, Yasufumi Shigeyoshi⁵ and Hiroki R. Ueda^{1,2,3,9}

Singularity behaviour in circadian clocks^{1,2} — the loss of robust circadian rhythms following exposure to a stimulus such as a pulse of bright light — is one of the fundamental but mysterious properties of clocks. To quantitatively perturb and accurately measure the dynamics of cellular clocks^{3,4}, we synthetically produced photo-responsiveness within mammalian cells by exogenously introducing the photoreceptor melanopsin^{5–8} and continuously monitoring the effect of photo-perturbation on the state of cellular clocks. Here we report that a critical light pulse drives cellular clocks into singularity behaviour. Our theoretical analysis consistently predicts and subsequent single-cell level observation directly proves that desynchronization of individual cellular clocks underlies singularity behaviour. Our theoretical framework also explains why singularity behaviours have been experimentally observed in various organisms, and it suggests that desynchronization is a plausible mechanism for the observable singularity of circadian clocks. Importantly, these *in vitro* and *in silico* findings are further supported by *in vivo* observations that desynchronization underlies the multicell-level amplitude decrease in the rat suprachiasmatic nucleus induced by critical light pulses.

To synthetically produce photo-responsiveness, we transiently transfected mouse *melanopsin* complementary DNA^{5–8} into NIH3T3 mouse fibroblast cells (ref. 4; Fig. 1a). To evaluate the effect of photo-perturbation on the state of circadian clocks, the cells were also transfected with a plasmid containing luciferase driven by the promoter of the *PER2* clock gene (*PER2*-luciferase reporter) and stimulated with forskolin to synchronize circadian rhythmicity. We then monitored multicell-level

PER2-luciferase reporter activity in real time^{9,10}. About two days after forskolin stimulation, cells with or without melanopsin were exposed to a 6-h light pulse, and then evaluated for the effect on multicell-level *PER2*-luciferase reporter activity about one day after the light pulse (see Fig. 1b, in which the bioluminescence data were detrended by subtracting their baseline tendency (see Supplementary Information for the details)). Melanopsin-positive cells exhibited a 1.8-h phase advance and a 2.5-fold amplitude change in *PER2*-luciferase reporter activity induced by the light pulse compared with that of cells that had not been exposed (Fig. 1b, upper panel; Fig. 1c, red bars). By contrast, melanopsin-negative cells exhibited little phase shift or fold change in amplitude induced by the light pulse (Fig. 1b, lower panel; Fig. 1c, blue bars). These results clearly indicate that the light pulse can perturb the state of mammalian circadian clocks in a melanopsin-dependent manner. In addition, the administration of the intracellular calcium chelator BAPTA-AM (1–10 μ M) or PLC (phospholipase C) inhibitor U73122 (0.1–3 μ M) into medium 1 h before light-pulse exposure inhibited the phase advance induced by the light pulse in a dose-dependent manner (see Supplementary Information, Fig. S1), indicating that PLC-mediated intracellular Ca²⁺ release is crucial for melanopsin-dependent photo-perturbation of mammalian clock cells.

To systematically quantify the phase shifts induced by light pulses of various timings and durations, high-throughput continuous monitoring of *PER2*-luciferase reporter activity was employed^{9–11}. Twelve sets of melanopsin-positive and -negative cells were prepared and stimulated with forskolin every 2 h over a 24-h period. About 3 days after the first forskolin stimulation, melanopsin-positive and -negative cells were exposed to a light pulse and then evaluated for its effect on multicell-level *PER2*-luciferase reporter activity. These experiments were repeated using light pulses

¹Laboratory for Systems Biology and ²Functional Genomics Unit, Center for Developmental Biology, RIKEN, 2-2-3 Minatojima-minamimachi, Chuo-ku, Kobe, Hyogo 650-0047, Japan. ³Department of Bioscience, Graduate School of Science, Osaka University, Toyonaka, Osaka 560-0043, Japan. ⁴Research Fellow of Japan Society for the Promotion of Science. ⁵Department of Anatomy and Neurobiology, Kinki University School of Medicine, 377-2 Ohno-Hagashi, Osaka-Sayama, Osaka 589-8511, Japan. ⁶Division of Biological Science, Graduate School of Science, Nagoya University and CREST & SORST, Japan Science and Technology Corporation, Furo-cho 1, Chikusa, Nagoya 464-8602, Japan. ⁷COE Unit of Circadian Systems, Division of Molecular Genetics, Department of Biological Sciences, Nagoya University Graduate School of Science, Furo-cho, Chikusa-ku, Nagoya, 464-8602, Japan. ⁸Department of Cell Biology and Neuroscience, Osaka University Graduate School of Medicine, 2-2 Yamadaoka, Suita, Osaka, 565-0871, Japan.

⁹Correspondence should be addressed to H.R.U. (uedah-tky@umin.ac.jp)

¹⁰These authors contributed equally to this work.

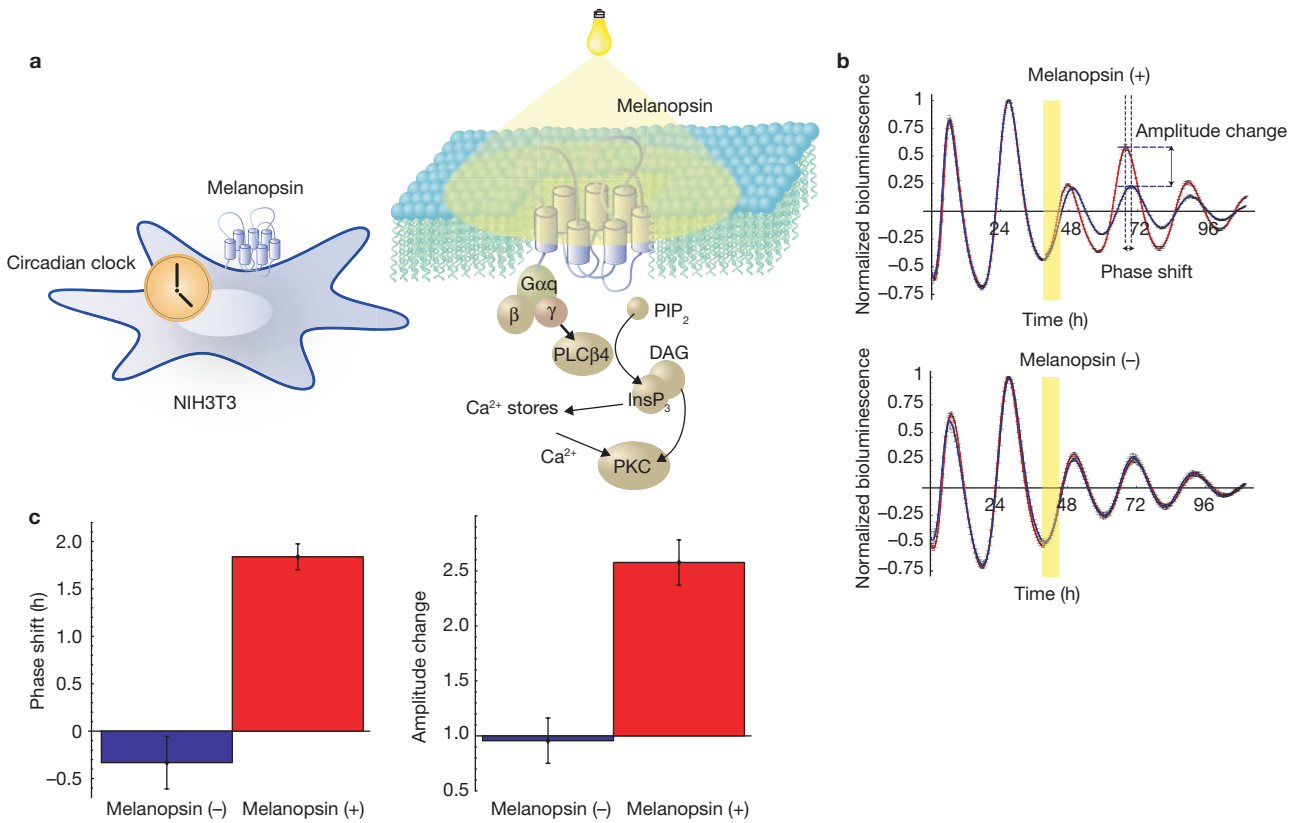


Figure 1 Synthetic implementation of photo-responsiveness within mammalian clock cells. **(a)** A diagram showing melanopsin-dependent photo-responsive NIH3T3 cells, and the known Gq signalling pathway⁸. Melanopsin-coupled Gq proteins stimulate phospholipase C (PLC). Active PLC hydrolyses phosphatidylinositol 4,5-bisphosphate (PIP₂) to produce inositol triphosphate (InsP₃) and diacylglycerol (DAG). These secondary messengers then activate protein kinase C (PKC), either directly (DAG) or indirectly through the release of internally stored calcium (InsP₃). **(b)** Photo-responsiveness of multicell-level PER2-luciferase reporter

activities of melanopsin-positive and -negative cells. The multicell-level bioluminescence data from the cells with (red) and without (blue) light-pulse exposure has been detrended (the baseline tendency has been removed) and then normalized by the level of the last peak before the light pulse (yellow) for comparison (see Supplementary Information for details of data processing). The phase shift (advance) and amplitude change (increase) of melanopsin-positive cells induced by the light pulse are indicated in the upper panel. **(c)** Quantification of the phase shifts and the fold changes in amplitude of the melanopsin-positive (red) and -negative (blue) cells induced by light pulse.

of different durations including 0.5, 1, 3, 6 and 12 h. To quantify the phase shift, we extracted the oscillatory components of detrended bioluminescence data (see Supplementary Information for the details). As shown in Fig. 2a and b, phase shifts induced by light pulses depended on the timing of light pulse. We then calculated multicell-level phase response curves (PRCs), where phase shifts are plotted against the timing of light pulses (Fig. 2c). The calculated PRCs for all tested durations show that the transition from phase advance to phase delay is around circadian time (CT)~6 (subjective noon), whereas the reverse transition is around CT~17 (near subjective midnight). Similar phase shifts were observed in *BMAL1*-luciferase reporter activity (see Supplementary Information, Fig. S2), suggesting that melanopsin-dependent photo-perturbation can control the core components of mammalian circadian clocks¹⁰. Notably, these multicell-level PRCs resemble light-type PRCs observed in mammals at the organism level^{12,13} (see Supplementary Information for details).

In addition to inducing phase shifts, light pulses can also increase or decrease the amplitude of *PER2*-luciferase reporter activity (Fig. 3a, b) (see Supplementary Information for the details). We averaged the amplitude change during the two days after the light pulse to quantify the multicell-level amplitude response curves (ARCs), where multicell-level amplitude changes are plotted against the timing of light pulses (Fig. 3c).

All ARCs are continuous, and the maxima and minima of ARCs are located around CT~6 (subjective noon) and CT~17 (near subjective midnight), respectively. Moreover, the maximum and minimum values of the ARCs depend on the light duration. On the basis of these results, we conclude that the phase and amplitude of mammalian cellular clocks can be adjustably and quantitatively controlled by melanopsin-dependent photo-perturbation.

From the ARCs, we found that a 3-h light pulse applied at CT~17 significantly decreased the amplitude of *PER2*-luciferase reporter activity at the multicell level. By conducting photo-perturbation of cellular clocks with 3-h light pulses delivered at around CT~17 at high temporal resolution (see Supplementary Information, Fig. S3), we found a critical light pulse capable of driving cellular clocks into singularity behaviour where robust multicell-level *PER2*-luciferase reporter activity was abolished (Fig. 4a). Because the circadian oscillation is recovered by a second light pulse applied about 3 days after the first one (Fig. 4a), we confirmed that the clocks or cells themselves are not impaired permanently, but only stopped transiently by the critical light pulse, suggesting that this multicell-level singularity behaviour holds the same properties as those already observed at the multicell level in populations of unicellular organisms or multicellular organisms¹⁴.

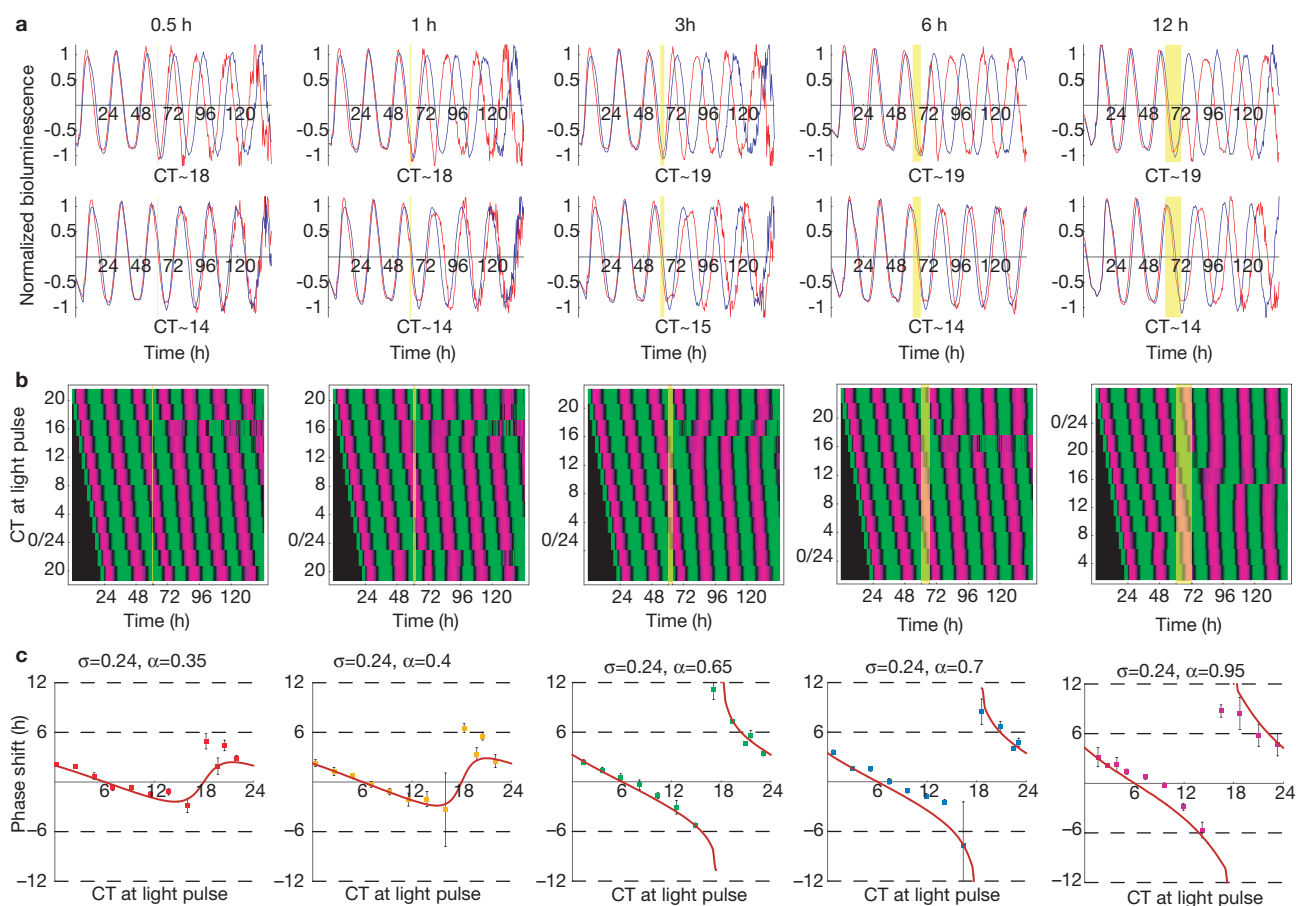


Figure 2 Phase shift of mammalian clocks induced by photo-perturbation. (a) Phase advance (upper panels) and delay (lower panels) induced by light pulses of different durations. The oscillatory components of *PER2*-luciferase reporter activities of melanopsin-positive (red) and -negative (blue) cells (see Supplementary Information for details of data processing) are shown with light pulses (yellow). The timing and duration of light pulses are as designated in each panel. (b) High-throughput analysis of phase shifts induced by light pulses (yellow) of various timings and durations. Magenta

and green denote high and low oscillatory components of *PER2*-luciferase reporter activities. (c) Phase-response curves (PRCs) of the *PER2*-luciferase reporter activities of melanopsin-positive cells against the timings of light pulses in circadian time (CT). Simulated PRCs by using the multiple cellular clock model are shown in red curves. Bioluminescence data of the negative control experiment using melanopsin (-) cells as well as the superimposition of five PRCs induced by different durations of light pulses are shown in the Supplementary Fig. S9.

Two alternative single-cell-level mechanisms have been proposed for this multicell-level singularity behaviour. The first is arrhythmicity or suppression of amplitude of individual clocks (Fig. 4b, upper panel) and the second is desynchronization of individual rhythmically oscillating clocks (Fig. 4b, lower panel)^{1,2}. Although both mechanisms are based on the limit-cycle model for circadian clocks^{1,2}, where circadian oscillation is represented as an attractive closed orbit, there is a fundamental difference between the dynamic scenarios of these mechanisms (see Supplementary Information for the details). The former mechanism relies on a simple limit-cycle model in which an unstable fixed point, called the 'singularity point', exists within the single limit-cycle orbit. Limit-cycle oscillation will be stopped once it is brought to this point by an external perturbation at the appropriate timing and strength. In this dynamic scenario, singularity behaviour observed at the multicell level is predicted to be caused by arrhythmicity of all individual cellular clocks^{1,2}. With the increasing number of reports on singularity behaviours in various organisms, this hypothesis has come to predominate to the point that the observed behaviour is named after the singularity point of the limit cycle.

By contrast, the second mechanism predicts that the singularity behaviour observed at the multicell level is due to the desynchronization of individual cellular clocks induced by critical perturbation^{1,2}. This scenario can also be explained by a limit-cycle model, especially in the presence of substantial fluctuations among individual cellular clocks. If such fluctuations exist, most of the circadian oscillators brought to the unstable fixed point cannot stay at this point for a long time, and therefore quickly return to the original orbit. The phases of the oscillators after recovery can vary greatly because small differences in the phases will be amplified by passing near the unstable fixed point, where all possible phases are defined theoretically. Thus, when stimuli are applied to a set of cellular circadian clocks at the appropriate timing and strength, the clocks can become desynchronized as the result of amplification of internal fluctuations in the state of cells or external fluctuations in the applied stimulus, leading to apparent arrhythmicity or suppression of amplitude in the averaged behaviour of the clocks at the multicell level. Arthur T. Winfree supported the second mechanism (desynchronization) on the basis of his experimental data¹, whereas the first scenario has gained wide acceptance as the main explanation for observed singularity behaviours although the underlying mechanism has not been directly verified at the single-cell level.

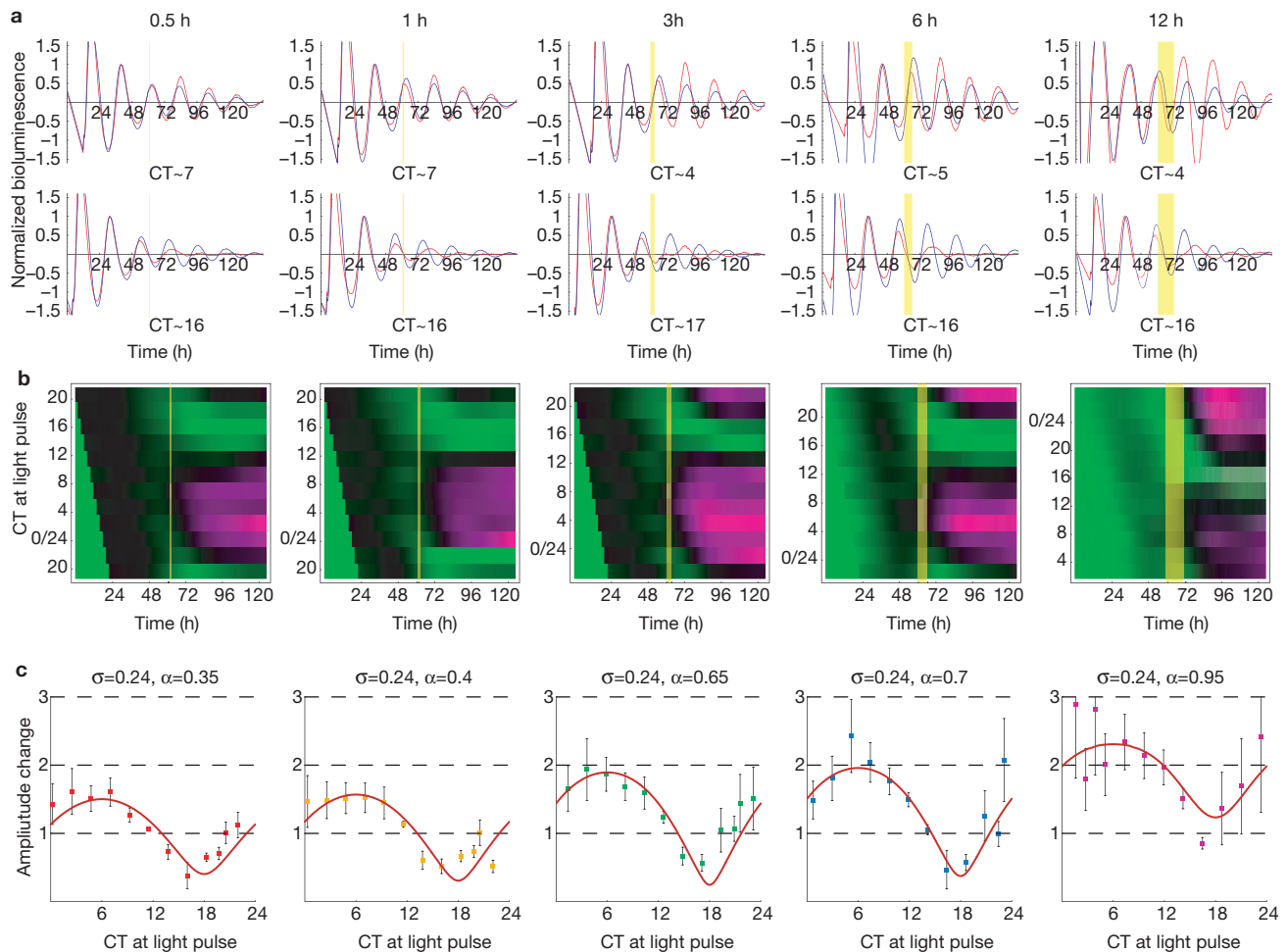


Figure 3 Amplitude changes of mammalian clocks induced by photo-perturbation. **(a)** Amplitude increase (upper panels) and decrease (lower panels) of *PER2*-luciferase reporter activities induced by light pulses (yellow) of different durations. The bioluminescence data from melanopsin-positive (red) and -negative (blue) cells were detrended (the baseline tendency has been removed) and normalized as in Fig. 1b. **(b)** High-throughput analysis of fold changes in amplitude induced by light pulses (yellow) of various

timings and durations. Magenta and green denote high and low normalized amplitudes of *PER2*-luciferase reporter activities. The fold-change in amplitude is obtained by data processing of the original bioluminescence data (see Supplementary Information for details of data processing). **(c)** Amplitude response curves (ARCs) of the *PER2*-luciferase reporter activities of melanopsin-positive cells against the timings of light pulses in CT. Simulated PRCs by the multiple cellular clock model are shown in red curves.

To directly verify these predictions at a single-cell level, we measured *PER2*-luciferase reporter activity in individual cells^{11,15}. As reported previously^{15,16} and also shown in Fig. 4c, d, left panels, the phases of melanopsin-negative cells gradually diverge over time independently of the stimulus (Fig. 4c, d, left panels and see Supplementary Information, Movie 1), which is consistent with a multicell-level decrease in amplitude. By contrast, when melanopsin-positive cells are exposed to a critical light pulse capable of inducing the singularity behaviour, the phases of cells are abruptly diversified by the pulse (Fig. 4c, d right panels, Supplementary Information, Fig. S5, and Supplementary Information, Movie 2), suggesting that desynchronization was induced by the light pulse. To exclude the possibility that this diversification of phase might be due to arrhythmic behaviour of individual cells, we tried to verify that the oscillation is regularly sustained after the light pulse by rearranging the order of cells in Fig. 4d according to the timing of the third peaks of individual cells (Fig. 4e). We observed that the single-cell-level oscillations of melanopsin-positive cells were sustained after the light pulse, and that the onset of those single-cell-level oscillations was within one day of the light pulse

for most of the individual cells, indicating that the observed singularity behaviour cannot be attributed to the arrhythmicity of individual cells. In addition, we verified that the critical light pulse induced no significant changes in single-cell-level amplitude (see Supplementary Information, Figs S4, S5), which excludes the possibility that the multicell-level amplitude decrease could be simply attributed to the single-cell-level amplitude decrease. Given these findings, we conclude that desynchronization of cellular clocks underlies the multicell-level singularity behaviour.

Although we have experimentally verified desynchronization of cells near the phase divergence (CT~17) points of the PRC, it remained unknown whether this single-cell-level mechanism can consistently explain the multicell-level phase shifts and amplitude changes observed for light pulses of various timing and duration. To address this question, we firstly verified that synchronization of cells can be induced by a light pulse near the convergence point of the PRC (CT~6), demonstrating that a multicell-level amplitude increase can be caused by synchronization of cell phases (see Supplementary Information, Fig. S5b, c). In addition, we constructed a mathematical model for multiple

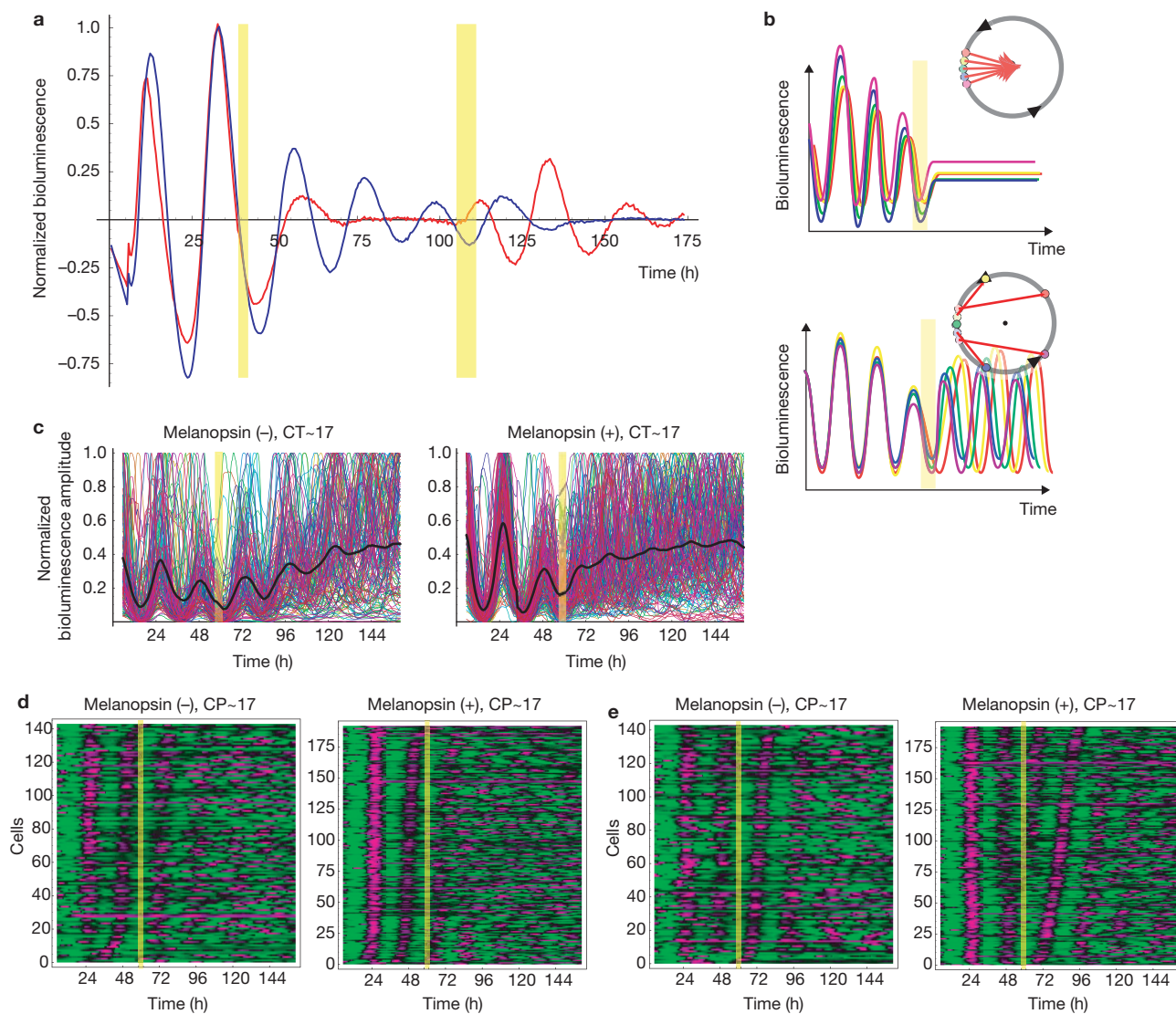


Figure 4 Desynchronization underlying the singularity behaviour of mammalian clocks. **(a)** Singularity behaviour of mammalian circadian clocks. Robust circadian rhythmicity of mammalian clocks is abolished after the first light pulse, and recovered by the second light pulse. The detrended (the baseline tendency has been removed) and normalized *PER2*-luciferase reporter activities of melanopsin-positive (red) and -negative (blue) cells are displayed with light pulses (yellow). **(b)** Schematic diagrams of two alternative single-cell-level mechanisms for the multicell-level singularity behaviour; arrhythmicity (upper panel) and desynchronization (lower panel) of individual

cellular clocks (see Supplementary Information for details) to evaluate multicell-level PRCs and ARCs on the basis of single-cell level dynamics. As shown in Figs 2c and 3c, the model qualitatively reproduced the topology of PRCs and the maximum and minimum values of the ARCs as well as their detailed shapes observed in the experimental data. Moreover, the identified parameter value of phase variation ($\sigma=0.24$) was consistent with the values of phase variation ($\sigma=0.22\sim 0.26$) estimated from the single-cell-level measurement. Given these findings, we concluded that the proposed single-cell-level mechanism of the singularity behaviour is capable of consistently explaining the multicell-level light response of mammalian circadian clocks.

cellular clocks. **(c)** The normalized *PER2*-luciferase reporter activities from individual cells with their averages (black thick lines) (see Supplementary Information for details of data processing). The timing of the light pulse (yellow) is designated in each panel. *PER2*-luciferase reporter activities from randomly selected representative cells were shown in Supplementary Fig. S4. **(d, e)** The detrended and normalized *PER2*-luciferase reporter activities from individual cells (see Supplementary Information for details of data processing). Magenta and green denote high and low bioluminescence. The data are sorted by the timing of the second peaks **(d)** and that of the third peaks **(e)**.

To further extend our *in vitro* and *in silico* findings, we next investigated their *in vivo* relevance to examine whether desynchronization underlies the multicell-level amplitude decrease in mammalian central clocks (suprachiasmatic nucleus; SCN) induced by critical light pulses. To quantify expression of clock genes in the rat SCN after the critical light pulses, rats were entrained under light–dark conditions (LD) for 2 weeks followed by 1 day in constant darkness (DD), exposed to the critical light pulses (two sequential 12-h light pulses started from CT16) and then kept in the DD condition. Rats were exposed to multiple light pulses, on the basis that a similar experiment produced singularity behaviours in humans¹⁷, where multiple sequential light pulses were applied to induce strong (type 0) phase shifts and, hence, singularity

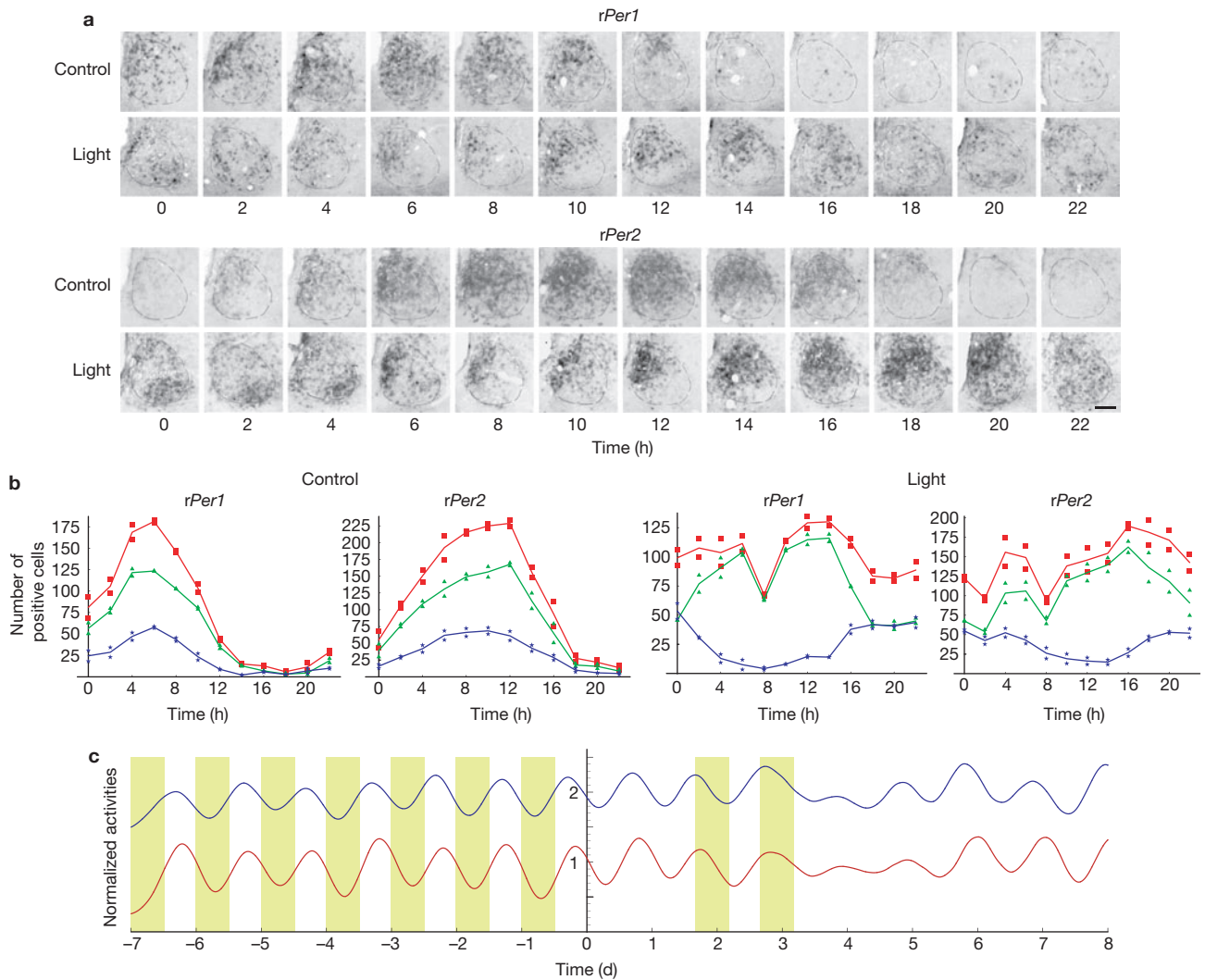


Figure 5 Desynchronization underlying the multicell-level amplitude decrease in the rat suprachiasmatic nucleus (SCN) induced by the critical light pulses. **(a)** Spatio-temporal expression of *Per1* and *Per2* genes in the rat SCN examined by *in situ* hybridization using a digoxigenin-labelled *Per1* and *Per2* cRNA probes. Upper and lower panels indicate the expression of *Per1* (upper) and *Per2* (lower) genes in the SCN with (light) or without (control) the critical light pulses. The left side of each figure is the medial side of the SCN. Dashed lines indicate the SCN boundaries. The bar indicates 100 μm . **(b)** Number

of positive cells in the entire SCN (red), dorsomedial (DM) region (green) and ventrolateral (VL) region (blue). Each point corresponds to data from one SCN sample, and the curves are the linear interpolations of the averages of two independent rats samples. **(c)** Time series of the locomotor activities of two independent rats who showed substantial decrease in amplitude of locomotor activity one day after the critical light pulses. To extract long-term trend of locomotor activity, we applied moving average with 4-h window size three times to the original locomotor activity data collected every 5 min.

behaviours. In humans¹⁷ and rats (this study), a single light pulse could induce only weak (type 1) phase shifts. Expression of *Per1* and *Per2* genes in the SCN in rats detected by *in situ* hybridization exhibit a remarkable multicell-level amplitude decrease after the critical light pulses (Fig. 5a, b, red lines). Importantly, this multicell-level amplitude decrease in the SCN is correlated with the spatially desynchronized expression pattern of *Per1* and *Per2* within the SCN observed between dorsomedial (DM) and ventrolateral (VL) regions (Fig. 5b, green and blue lines). The observed spatial desynchronization was also verified more locally by using a computer program that can automatically analyse the intensities of sequential SCN slice images at the pixel level (see Supplementary Information, Fig. S6 and Supplementary Information for details).

Under the same experimental condition, we also confirmed that the critical light pulses can induce the temporal amplitude decrease of locomotor activity in a substantial portion of rats (30%) about

1 day after the second light pulse (Fig. 5c). This percentage of observed temporal amplitude decrease is comparable to, or even higher than, the previous observations in other mammalian organisms (~20% both in chipmunk¹⁸ and human¹⁷). As in the case of other organisms, the temporal amplitude decrease of locomotor activity is strongly dependent on the timing of light pulses, because the reductions in amplitude were induced only by light pulses applied near CT16 (data not shown). These results suggest that the critical light pulse used in this experiment can also predispose an organism to the temporal amplitude decrease of locomotor activity *in vivo*.

There are differences between our *in vitro* system and *in vivo* organisms. First, our melanosin-positive NIH3T3 cells seem to lack cell–cell coupling, whereas the SCN has cell–cell communication. Second, light directly hastens desynchrony in our *in vitro* system, whereas it is presumed to initiate transient desynchrony *in vivo* indirectly through retinal

projections to the *in vivo* SCN. Thus, the interpretation that desynchronization seen in our *in vitro* system is relevant to that of the *in vivo* SCN depends on the assumptions that (1) substantial fluctuations exist in the states of SCN clock cells^{19,20}, and that (2) the phase shifts in our *in vitro* system induced directly by light is basically the same as those in SCN evoked indirectly by light (Fig. 2), those of which seem valid at least in mammals (see Supplementary Information for details).

In other organisms, we expect that the desynchronization of individual circadian oscillators will underlie the singularity behaviour. The simple limit-cycle model predicts that the singularity behaviour can be induced merely by the infinitesimal range of perturbation strength and timing, which stands in sharp contrast to the reproducible observations of singularity behaviours in various organisms. By contrast, our multiple cellular clock model predicts that the multicell-level singularity behaviour will be robustly induced by the experimentally achievable range of perturbation strength and timing (green regions in Supplementary Information, Fig. S7) if there are substantial fluctuations in the state of individual cellular clocks. Because recent single-cell level measurement of individual cellular clocks in the SCN revealed substantial fluctuations in the states of central clocks^{19,20}, our model predicts that desynchronization of cellular clocks in the SCN can be stably induced by the critical light pulses, which is quite consistent with our robust observations that the desynchronization actually underlies the multicell-level amplitude decrease in the SCN after the critical light pulses that can also probabilistically induce temporal amplitude decrease of locomotor activity.

Although we suggest desynchronization as a plausible and general mechanism for singularity behaviours not only in mammalian and other organisms, we cannot completely exclude the possibility that arrhythmicity of individual clocks might underlie singularity behaviours in other organisms because various extended models of singularity behaviour have been proposed^{21–23}. In the investigation of singularity behaviours in such systems, the direct verification by single-cell level measurement and quantitative perturbation will play a crucial part in determining the underlying mechanism as demonstrated in this report. □

METHODS

Plasmid construction. Plasmid construction protocols are provided in the Supplementary Information.

Cloning of full-length mouse *melanopsin* (*Opn4*) cDNA. We prepared total RNA from C57BL/6 mouse eyes using TRIzol reagent (Invitrogen, Carlsbad, CA). A cDNA library was synthesized from total RNA using pd(T)_{12–18} (GE Healthcare, Chalfont, UK) and SuperScriptII Reverse Transcriptase (Invitrogen) according to the standard protocol. The full-length coding sequence of *melanopsin* was amplified from the cDNA library by polymerase chain reaction with a forward primer containing the I-SceI recognition sequence and a reverse primer containing the PI-PspI recognition sequence. PCR product was digested with I-SceI and PI-PspI, cloned into the pMU2-P(*GAPDH*)-control vector, and termed pMU2-P(*GAPDH*)-*melanopsin*. *melanopsin*-forward:5'-ATTACCCTGTTATCCCTAATGACTCTCCTTCAGGACCAAG-3'. *melanopsin*-reverse:5'-ACCCATAATACCATAATAGCTGTTGCCACAGATGTCTGAGAGTCACATC-3'.

High-throughput real-time *PER2*- and *BMAL1*-luciferase-reporter assays. High-throughput real-time *PER2*- and *BMAL1*-luciferase reporter assays were performed as described previously¹¹ with the following modifications. NIH3T3 cells (American Type Culture collection, Manassas, VA) were grown in Dulbecco's modified Eagle's minimal essential medium (DMEM) supplemented with 10% fetal bovine serum (FBS; JRH Biosciences, Lenexa, KS) and antibiotics (25 units ml⁻¹ penicillin, 25 µg ml⁻¹ streptomycin; GIBCO, Carlsbad, CA). Cells were plated at 2×10⁵ cells per 35-mm dish 24 h before transfection. Transfection was carried out with FuGene6

(Roche Applied Science, Indianapolis, IN) according to the manufacturer's instructions, and cells in each dish were transfected with 5 µg of plasmid (1 µg of *PER2*- or *BMAL1*-luciferase reporter plasmids and 4 µg of pMU2-P(*GAPDH*)-control or -*melanopsin*). After 72 h, the medium in each well was replaced with 2 ml of culture medium (DMEM, 10% FBS) supplemented with 10 mM HEPES (pH 7.2), 0.1 mM luciferin (Promega, Madison, WI), antibiotics, and 0.01 µM forskolin (Nacalai Tesque, Kyoto, Japan). Cells were maintained in complete darkness except for brief exposure to weak red light. Bioluminescence was measured using a photomultiplier tube (PMT) detector assemblies (Hamamatsu Photonics, Shizuoka, Japan). The modules and cultures were maintained in a darkroom at 30 °C and interfaced with computers for continuous data acquisition. Light pulses were generated by a 100-W tungsten source, filtered with far-infrared cut filter, and calibrated by a radiometer (LI-250A Light Meter; LI-COR Biosciences, Lincoln, NE). The intensity of light pulse was set to 3.0 µM s⁻¹ m⁻² before individual experiments. Photons were counted for 2 min at 24-min intervals. The protocols for pharmacological assays and the methods for bioluminescence data analysis are provided in the Supplementary Information. In this protocol, we started with the forskolin stimulation followed by the quantitative melanopsin-mediated stimulation. Although melanopsin cells can be directly entrained by sequential light-dark cycle (H. U., T.J.K. and H.R.U., unpublished data), the phase shift induced by melanopsin-mediated stimulation seems weaker than that of forskolin-mediated stimulation in our cellular system. A single forskolin-stimulation can generate quantitatively reproducible circadian oscillations in our system despite presumable experimental fluctuations in pre-culture, and enables us to define the good reference time point (circadian time 0) as the timing of forskolin stimulation. Thus, we combined these two stimulations in order to maximize the reproducibility and quantitiveness in our experiments. The detailed information on the number of cultures and repeated experiments is shown in Supplementary Information, Table S1.

Real-time single-cell bioluminescence imaging. Samples were prepared as described previously in high-throughput real-time reporter assay except for the use of pGL4-*PER2-Luc* reporter plasmid¹¹. 35-mm culture dishes were sealed with cover slips, placed on the stage of a luminescence microscope (Luminoview, LV100, Olympus, Tokyo, Japan), and kept at 30 °C in a heated chamber (Olympus). Bioluminescence was imaged using a 10× objective (LUCPlanFLN 10, Olympus, NA 0.3) and transmitted to a cooled CCD camera (ORCA-II ER, Hamamatsu Photonics) mounted on the bottom port of the microscope. Readout noise was reduced by using 4×4 binning of the 336×256 pixel array. Time-lapse images were collected at 30-min intervals with 25-min exposures by a computer using image analysis software (Metamorph, Universal Imaging Corp., Ontario, Canada). The light pulse was applied by opening the shutter for bright-field illumination with the intensity of 3.0 µM s⁻¹ m⁻². The light pulse was filtered with far-infrared cut filter and calibrated by a radiometer. During the light-pulse exposure, the image collection was stopped, and then restarted following light-pulse exposure.

Image processing for real-time single-cell bioluminescence imaging. Images were corrected for bias and dark current by subtracting a background image using Matlab (MathWorks, Natick, MA). Hot pixels and cosmic rays were removed by applying the spatial and temporal local median filters, respectively. The positions of the hot pixels were detected by measuring the dark image. The cosmic rays were detected by comparing the intensities of pixels for the temporally adjacent images. Supplementary movies were then created with Metamorph (Ontario, Canada). The bioluminescence of each cell was estimated from the average of the top ten maximum pixels within the region of interest manually defined for each cell by a custom-made software program developed with Matlab. Before the estimation, the spatial Gaussian filter was applied to avoid counting noise pixels. Remaining data processing of the obtained single-cell bioluminescence data was conducted with Mathematica (Wolfram Research, Champaign, IL). The methods for single-cell bioluminescence data analysis are provided in Supplementary Information.

Animals and housing. Adult male Wistar rats (JAPS, Osaka, Japan) were purchased 5 weeks after birth. Rats were housed on a 12-h light (400 lux): 12-h dark (LD12: 12) cycle (light on at Zeitgeber time 0 (ZT0), and light off at ZT12), and were given food and water *ad libitum*. Rats were maintained under these lighting conditions for at least 2 weeks. On Day 0, animals were transferred to constant darkness (DD) for one day, and on the first day (Day1) and the second day (Day 2) they were exposed to a 12-h fluorescent light (400 lux) from circadian time

16 (CT16) to CT4. After the light exposure, rats were transferred to DD conditions. Brain samples were collected during the DD cycle on Day 0 or during the first entire DD cycle after the light exposure (Day 4) every 2 h. This study was performed in compliance with the Rules and Regulations of the Animal Care and Use Committee, Kinki University School of Medicine, and in strict compliance with the Guide for the Care and Use of Laboratory Animals, Kinki University School of Medicine. The detailed information on the sampling timing for *in situ* hybridization is shown in Supplementary Information, Fig. S8.

***In situ* hybridization using digoxigenin-labelled probes.** Rats were deeply anesthetized with ether and intracardially perfused with 50 ml saline and 100 ml of a fixative containing 4% paraformaldehyde in 0.1 M phosphate buffer (PB), pH 7.4. Rat brain samples were postfixed in the same fixative for 24 h at 4 °C, soaked in PB containing 20% sucrose for 48 h and finally stored frozen at -70 °C. To examine the fine localization of messenger-RNA-expressing cells, cRNA fragments of rat *Per1* (nucleotides 736–1720) and *Per2* (nucleotides 1390–2915) were labelled with digoxigenin-UTP (Roche, Mannheim, Germany) by *in vitro* transcription with T7 RNA polymerase. Digoxigenin-labelled cRNA probes were synthesized using digoxigenin-UTP through the standard protocol for cRNA synthesis (Roche). The *in situ* hybridization method using digoxigenin-labelled probes was performed as described previously²⁴.

Stored tissues were cut to a thickness of 30 µm on the coronal plane using a cryostat and processed using the free-floating *in situ* hybridization method as described previously²⁵. Briefly, tissue sections were processed with 1 µg ml⁻¹ proteinase K (0.1 M Tris-HCl, pH 8.0, 50 mM EDTA) for 10 min at 37 °C, and 4% paraformaldehyde in 0.1 M PB for 10 min. Then sections were treated with 0.25% acetic anhydride in 0.1 M triethanolamine for 10 min and 2×SSC for 10 min. The sections were then incubated in hybridization buffer (60% formamide, 10% dextran sulphate, 10 mM Tris-HCl, pH 8.0, 1 mM EDTA, pH 8.0, 0.6 M NaCl, 0.2% *N*-laurylsarcosine, 0.2 mg ml⁻¹ transfer RNA, 1×Denhardt's, 0.25% sodium dodecyl sulphate and 10 mM dithiothreitol) containing *Per1* or *Per2* cRNA probe (20 ng per 100 ml) for 12 h at 60 °C. After two rinses in 2×SSC and 50% formamide at 60 °C, sections were treated with a solution containing 20 µg ml⁻¹ RNase A (10 mM Tris-HCl, pH 8.0, 1 mM EDTA, and 0.5 M NaCl) for 30 min at 37 °C. The sections were further washed in 2×SSC and 50% formamide and then in 0.4×SSC at 60 °C (30 min for each wash). They were then transferred into buffer 1 (100 mM Tris-HCl, pH 7.5 and 150 mM NaCl, room temperature, 5 min) and buffer 2 (1.5% blocking reagent added to buffer 1) for 1 h. They were further incubated overnight at 4 °C with alkaline-phosphatase-conjugated digoxigenin antibodies (Roche), diluted 1:1000 in buffer 1. On the following day, the sections were washed twice in buffer 1 (5-min each) and incubated in buffer 3 (100 mM Tris-HCl buffer, pH 9.5, containing 100 mM NaCl and 50 mM MgCl₂) for 3 min. Finally, they were incubated in a solution containing nitroblue tetrazolium salt (0.34 mg ml⁻¹) and 5-bromo-4-chloro-3-indolyl phosphate toluidinium salt (0.18 mg ml⁻¹) (Roche) for 16 h. The colouring reaction was stopped by immersing the sections in buffer 4 (10 mM Tris-HCl containing 1 mM EDTA, pH 8.0). The sections were analysed under a bright-field microscope. The methods for data processing of *in situ* hybridization images are provided in the Supplementary Information.

Behaviour analysis. To assess locomotor activity, rats were housed individually under the same experimental condition as in the *in situ* hybridization assays. The locomotor activity of an individual rat was recorded every 5 min by an area sensor (FA-05 F5B; Omron, Tokyo, Japan). To filter out noise and extract the long-term trend of locomotor activity, the moving average with 4-h window size was applied three times to the original locomotor activity data.

Note: Supplementary Information is available on the Nature Cell Biology website.

ACKNOWLEDGEMENTS

This research was supported by intramural Grant-in-Aid from the Center for Developmental Biology (CDB), Director's Fund from CDB (H.R.U.), KAKENHI (Grant-in-Aid for Scientific Research) on Priority Areas 'Systems Genomics' from the Ministry of Education, Culture, Sports, Science and Technology of Japan (H.R.U. and H.U.), Grant-in-Aid for Scientific Research on 'Development of Basic Technology to Control Biological Systems Using Chemical Compounds' from the New Energy and Industrial Technology Development Organization (NEDO) of Japan (H.R.U.) and Research Fellowships of the Japan Society for the Promotion of Science for Young Scientists 17-4169 (T.J.K.). We thank for Wataru Kishimoto for technical supports on high-throughput monitoring system, Rikuhiro G. Yamada

for support for data analysis, Maki Ukai-Tadenuma for technical support, Yoichi Minami for discussion for *in vivo* experiments, and Douglas Sipp Michael Royle, Danny Forger for critical comments on the manuscript. We also thank John J. Tyson for his suggestion regarding Winfree's original idea of desynchronization.

AUTHOR CONTRIBUTIONS

K.Y. and H.R.U. developed the concept of synthetic implementation of photo-responsiveness within NIH3T3 cells by using melanopsin. T.K. designed a high-throughput monitoring device. H.U. constructed all materials used in this work and performed high-throughput real-time luciferase reporter assays, single-cell real-time bioluminescence imaging and pharmacological assays. T.J.K. developed the theory, data-analysis methods, and the image-analysis software used in this work, analysed high-throughput, single-cell real-time bioluminescence, *in situ* hybridization, and locomotor activity data, and performed single-cell real-time bioluminescence imaging. M.N. and M.S. performed behaviour analysis of rats. M.N., K.M. and Y.S. performed *in situ* hybridization and analysed the data. H.U., T.J.K. and H.R.U. wrote the manuscript. All authors discussed the results and commented on the manuscript text.

Published online at <http://www.nature.com/naturecellbiology/>

Reprints and permissions information is available online at <http://npg.nature.com/reprintsandpermissions/>

- Winfree, A. T. Unclocklike behaviour of biological clocks. *Nature* **253**, 315–319 (1975).
- Winfree, A. T. *The Geometry of Biological Time* (Springer-Verlag, New York, 1980).
- Balsalobre, A., Damiola, F. & Schibler, U. A serum shock induces circadian gene expression in mammalian tissue culture cells. *Cell* **93**, 929–937 (1998).
- Akashi, M. & Nishida, E. Involvement of the MAP kinase cascade in resetting of the mammalian circadian clock. *Genes Dev.* **14**, 645–649 (2000).
- Melyan, Z., Tarttelin, E. E., Bellingham, J., Lucas, R. J. & Hankins, M. W. Addition of human melanopsin renders mammalian cells photoresponsive. *Nature* **433**, 741–745 (2005).
- Qiu, X. *et al.* Induction of photosensitivity by heterologous expression of melanopsin. *Nature* **433**, 745–749 (2005).
- Panda, S. *et al.* Illumination of the melanopsin signaling pathway. *Science* **307**, 600–604 (2005).
- Peirson, S. & Foster, R. G. Melanopsin: another way of signaling light. *Neuron* **49**, 331–339 (2006).
- Ueda, H. R. *et al.* A transcription factor response element for gene expression during circadian night. *Nature* **418**, 534–539 (2002).
- Ueda, H. R. *et al.* System-level identification of transcriptional circuits underlying mammalian circadian clocks. *Nature Genet.* **37**, 187–192 (2005).
- Sato, T. K. *et al.* Feedback repression is required for mammalian circadian clock function. *Nature Genet.* **38**, 312–319 (2006).
- Johnson, C. H., Elliott, J., Foster, R., Honma, K. & Kronauer, R. in *Chronobiology: Biological Timekeeping* (eds Dunlap, J. C., Loros, J. J. & DeCoursey, P. J.) 67–106 (Sinauer, Sunderland, Massachusetts, 2004).
- Johnson, C. H. Forty years of PRCs—what have we learned? *Chronobiol. Int.* **16**, 711–743 (1999).
- Johnson, C. H. & Kondo, T. Light pulses induce 'singular' behavior and shorten the period of the circadian phototaxis rhythm in the CW15 strain of *Chlamydomonas*. *J. Biol. Rhythms* **7**, 313–327 (1992).
- Welsh, D. K., Yoo, S. H., Liu, A. C., Takahashi, J. S. & Kay, S. A. Bioluminescence imaging of individual fibroblasts reveals persistent, independently phased circadian rhythms of clock gene expression. *Curr. Biol.* **14**, 2289–2295 (2004).
- Nagoshi, E. *et al.* Circadian gene expression in individual fibroblasts: cell-autonomous and self-sustained oscillators pass time to daughter cells. *Cell* **119**, 693–705 (2004).
- Jewett, M. E., Kronauer, R. E. & Czeisler, C. A. Light-induced suppression of endogenous circadian amplitude in humans. *Nature* **350**, 59–62 (1991).
- Honma, S. & Honma, K. Light-induced uncoupling of multioscillatory circadian system in a diurnal rodent, Asian chipmunk. *Am. J. Physiol.* **276**, R1390–R1396 (1999).
- Maywood, E. S. *et al.* Synchronization and maintenance of timekeeping in suprachiasmatic circadian clock cells by neuropeptidergic signaling. *Curr. Biol.* **16**, 599–605 (2006).
- Yamaguchi, S. *et al.* Synchronization of cellular clocks in the suprachiasmatic nucleus. *Science* **302**, 1408–1412 (2003).
- Leloup, J. C., Gonze, D. & Goldbeter, A. Limit cycle models for circadian rhythms based on transcriptional regulation in *Drosophila* and *Neurospora*. *J. Biol. Rhythms* **14**, 433–448 (1999).
- Leloup, J. C. & Goldbeter, A. A molecular explanation for the long-term suppression of circadian rhythms by a single light pulse. *Am. J. Physiol. Regul. Integr. Comp. Physiol.* **280**, R1206–R1212 (2001).
- Huang, G., Wang, L. & Liu, Y. Molecular mechanism of suppression of circadian rhythms by a critical stimulus. *EMBO J.* (2006).
- Yan, L., Takekida, S., Shigeyoshi, Y. & Okamura, H. *Per1* and *Per2* gene expression in the rat suprachiasmatic nucleus: circadian profile and the compartment-specific response to light. *Neuroscience* **94**, 141–150 (1999).
- Ban, Y., Shigeyoshi, Y. & Okamura, H. Development of vasoactive intestinal peptide mRNA rhythm in the rat suprachiasmatic nucleus. *J. Neurosci.* **17**, 3920–3931 (1997).

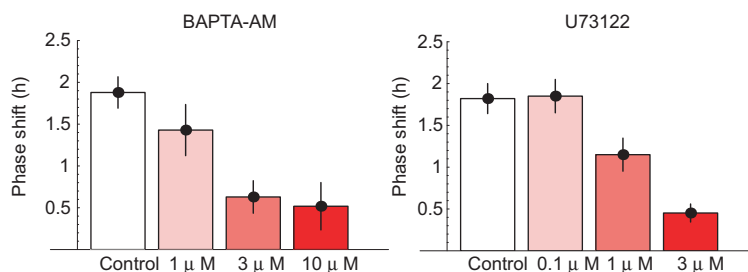


Figure S1 Dose-dependency of the phase shifts to drugs inhibiting intracellular Ca^{2+} signaling. Phase shifts of melanopsin-positive cells under the administration of drugs inhibiting intracellular Ca^{2+} signaling. The administration of intracellular calcium chelator BAPTA-AM (1–10 μM) or PLC inhibitor U73122 (0.1–3 μM) into medium 1 h before light-pulse exposure inhibited the phase advance induced by light pulse in a dose-dependent

manner, indicating that PLC-mediated intracellular Ca^{2+} release is critical for melanopsin-dependent photo-perturbation of mammalian clock cells. Error bars represent the standard deviations of the phase shifts. The doses are indicated in each panel. The protocols for pharmacological assays are provided in **Supplementary Methods**.

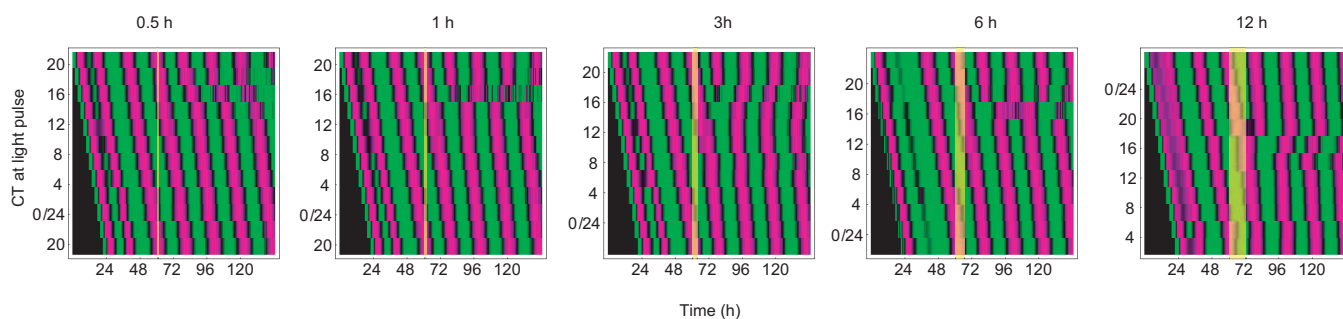


Figure S2 Phase shift of *BMAL1*-luciferase reporter activities induced by photo-perturbation. High-throughput analysis of phase shifts induced by

light pulses (yellow) with various timings and durations. Magenta and green denote high and low normalized *BMAL1*-luciferase reporter activities.

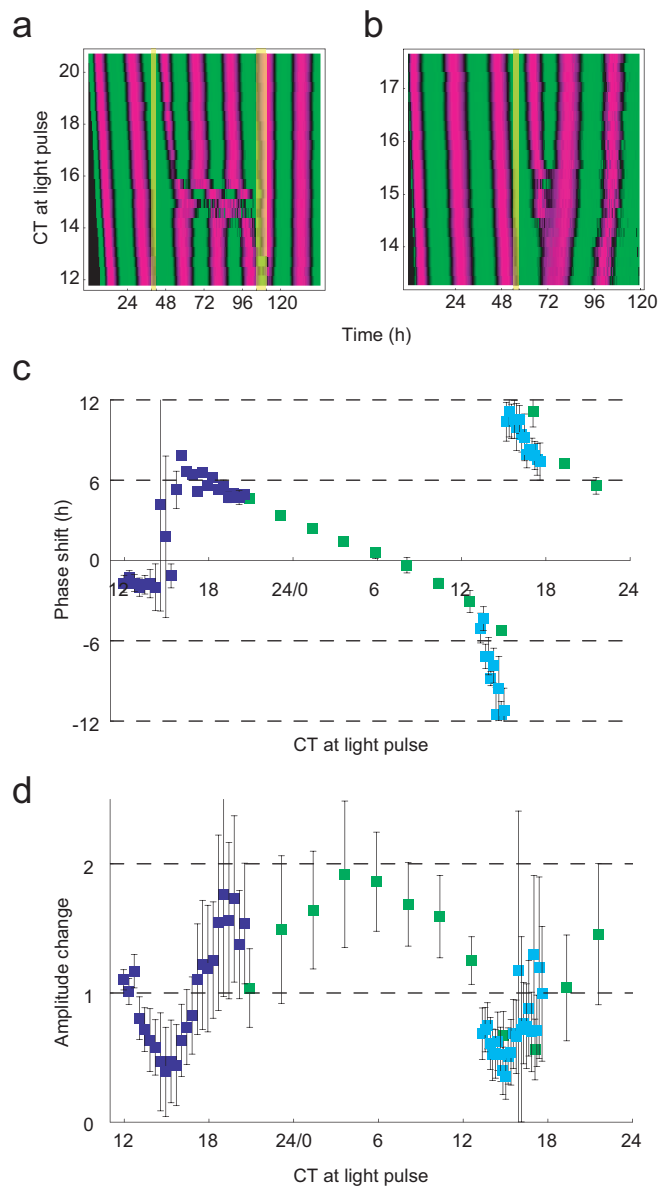


Figure S3 Phase shifts and amplitude changes induced by light pulse at high temporal resolution. (a and b) High-throughput analysis of phase shifts induced by light pulses (yellow) applied near CT~17 of the second day (a) or third day (b). Magenta and green denote high and low normalized

PER2-luciferase reporter activities. The intervals of light pulses are 20 min (a) and 10 min (b), respectively. (c and d) PRC (c) and ARC (d) for 3-hour light pulse near CT~17 of the second day (blue) or third day (cyan) at high temporal resolution. The data shown in green are the same as those in Figure 2c.

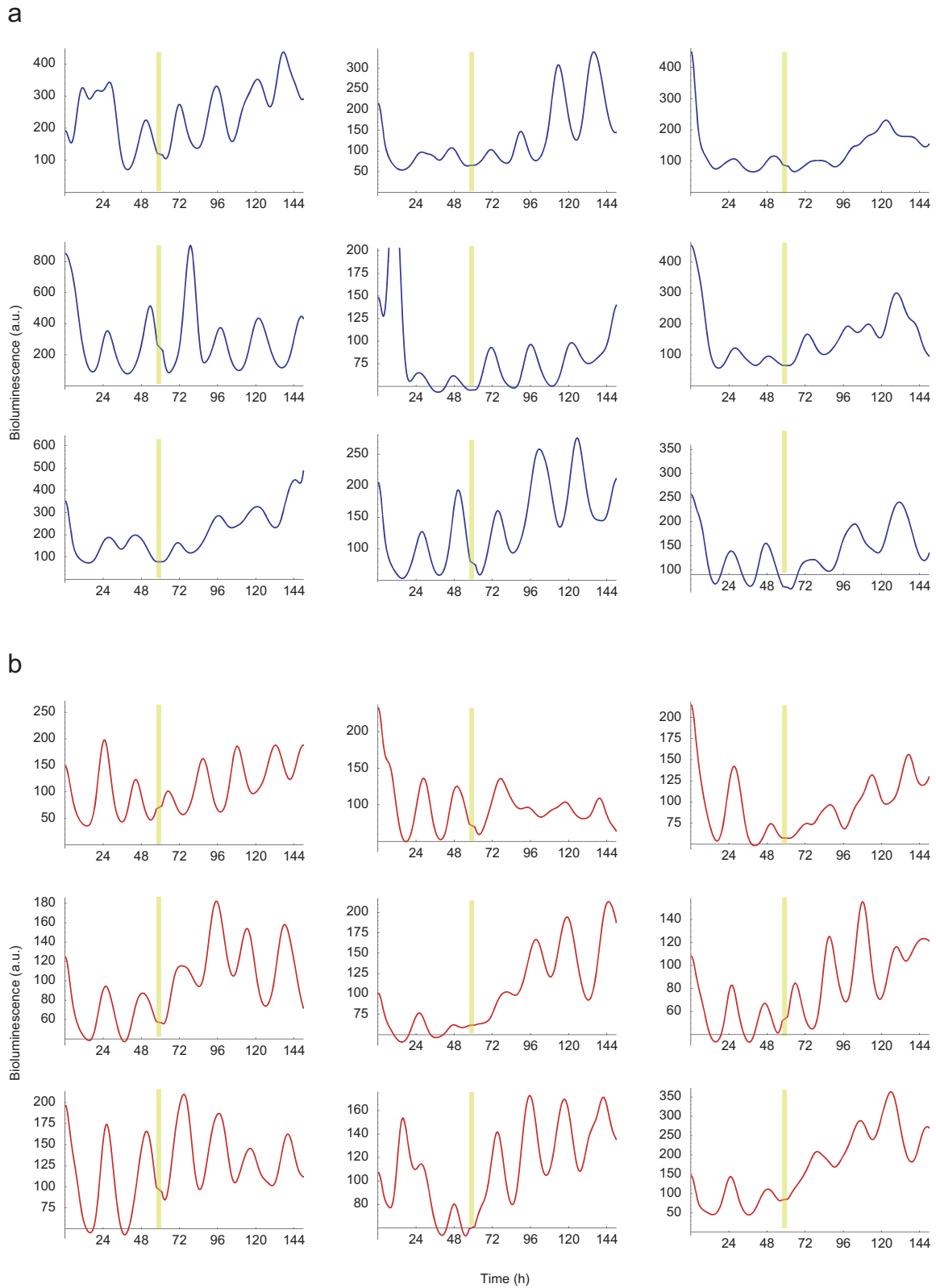


Figure S4 Single-cell-level circadian oscillations of nine representative cells. **(a and b)** Single-cell-level circadian oscillations of nine representative melanopsin-negative **(a)** and -positive **(b)** cells. Bioluminescence (a.u.) of individual cells measured by the single-cell bioluminescence imaging was

shown without normalization. The critical light pulse to induce multi-cell-level singularity was applied to both types of cells. The light pulse is shown in yellow. Nine cells were randomly chosen by a random number generator out of 192 **(a)** or 143 **(b)** cells.

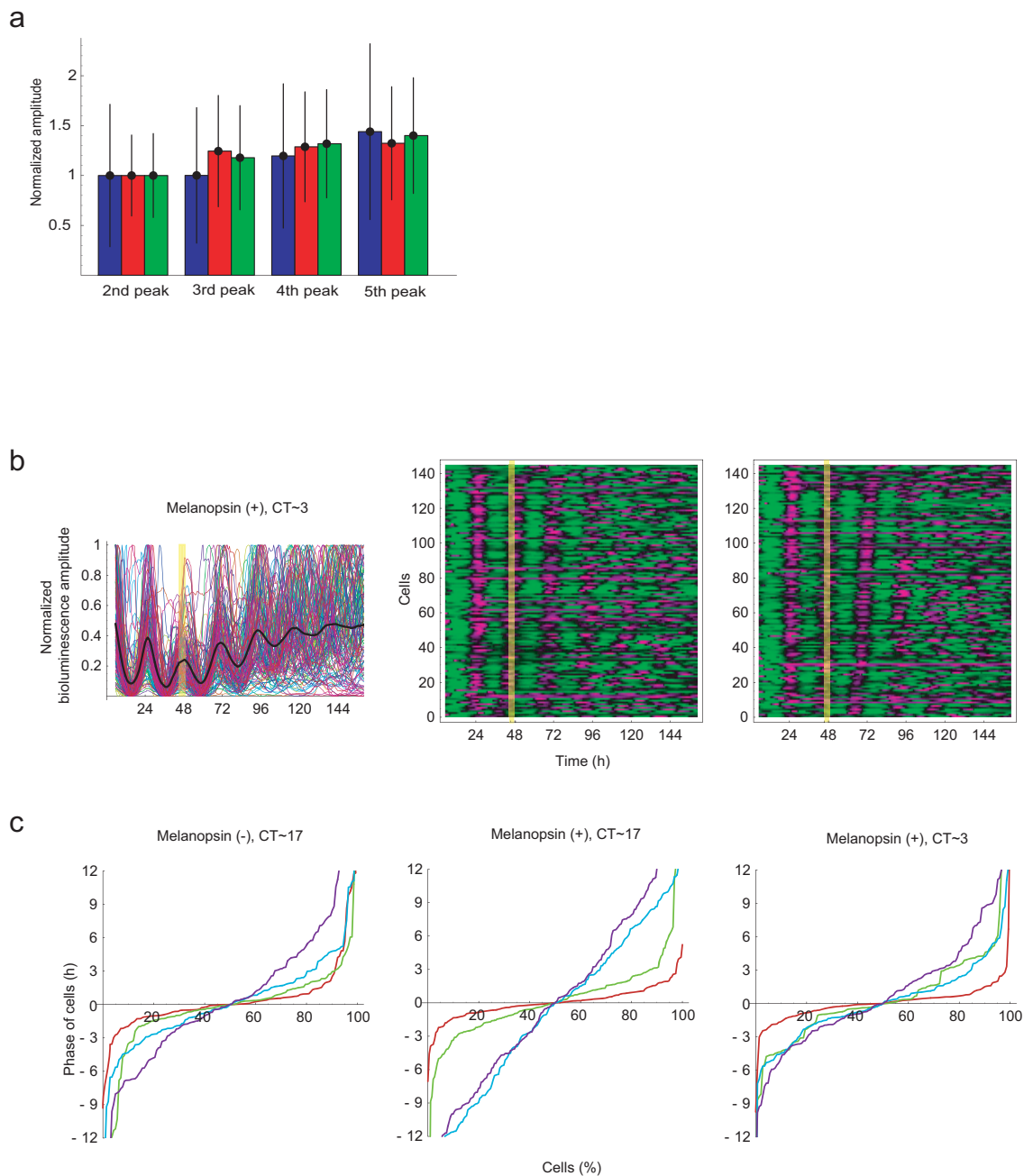


Figure S5 Single-cell-level amplitude change, and synchronization and desynchronization of cells by light pulses. **(a)** Average (filled bar) and standard deviation (error bar) of amplitude of 2nd, 3rd, 4th, and 5th peaks. The light-pulse has been applied about between 2nd and 3rd peaks. Blue bars represent the amplitude of melanopsin negative cells. Red and green bars represent the amplitude of melanopsin positive cells after the light-pulses inducing desynchronization (red) and synchronization (green), respectively. The average amplitudes were normalized by those of the 2nd peak for comparison. The first peak right after the forskolin stimulation was omitted here because it might be affected by forskolin stimulation. **(b)** The normalized *PER2*-luciferase reporter activities from individual cells (left panel) with their averages (black thick lines) and the detrended and normalized *PER2*-luciferase reporter activities from individual cells (middle and right panels). The timing of the light pulse (yellow) is designated in each panel. The data is sorted by the timing of the second peaks (middle panel) and that of the third peaks (right panel). **(c)** The cumulative plot of phase

for the first (red), second (green), third (blue), and fourth (purple) peaks (see **Supplementary Data** for details of data processing). The phases of cells are normalized so that their median value is zero. In this plot, the slope of each curve describes the variation of the phase. For example, a small slope represents that the phases of cells aggregate at their median phase, indicating synchronization of cellular clocks. On the other hand, a large slope represents that the phases of cells are broadly distributed, indicating the desynchronization of cellular clocks. Therefore, the gradual diversification of phases of the melanopsin-negative cells was represented in the cumulative plot of phase as the gradual increase in the slopes of the curves for the first, second, third, and fourth peaks (left panel). The abrupt divergence of phase of the melanopsin-positive cells after light pulse was described by the sharp increase in the slopes for the third peak (middle panel). The synchronization of phase was indicated by the no change in slopes for the second and third peaks (right panel).

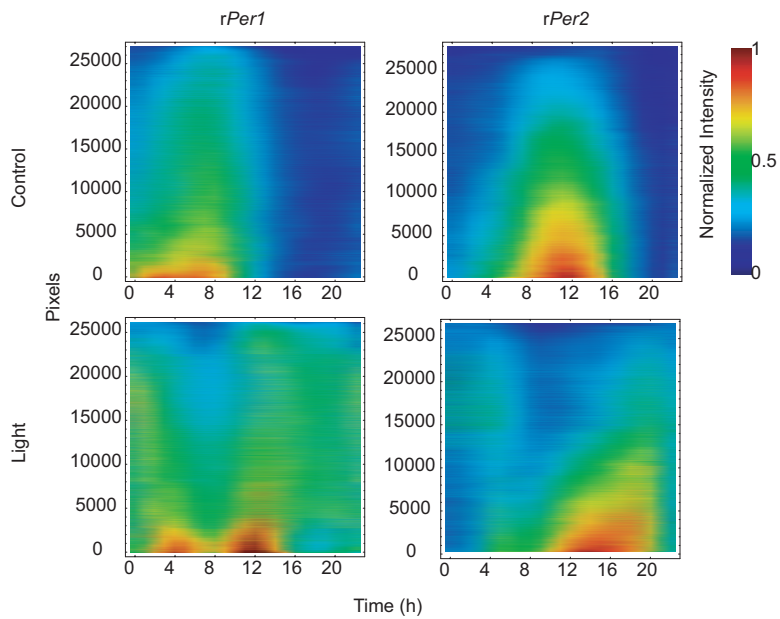


Figure S6 Time series of the normalized intensity of each pixel in the SCN images. The time series of pixels are sorted by their mean intensities so that

higher mean intensity corresponds to lower index (see **Supplementary Data** for details of data processing).

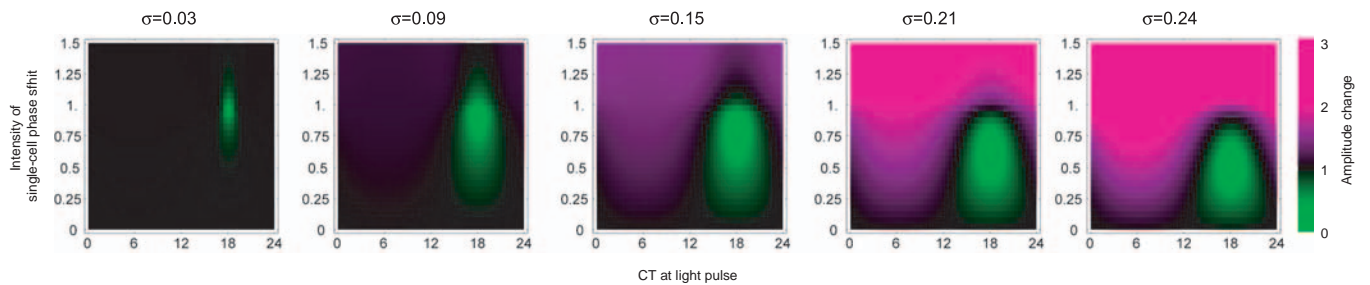


Figure S7 Simulated fold-changes in multi-cell-level amplitude as a function of the timing of light pulse and the intensity of single-cell-level phase shift. Each heatmap corresponds to the result for different phase variation before light pulse. Magenta and green denote increase and

decrease of multi-cell-level amplitude.

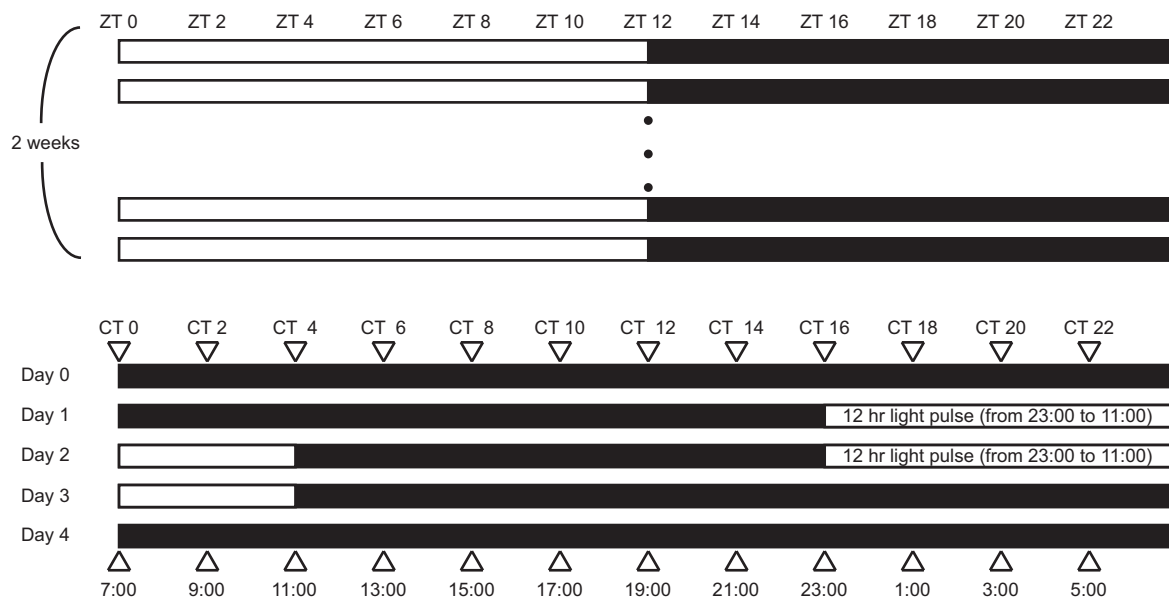


Figure S8 Sampling timings of rats for in situ hybridization. Rats maintained on the light/dark cycle [lights on at ZT0 (7 A.M.) and lights off at ZT 12 (7 P.M.)] for 2 weeks. On day 0, rats were transferred to constant darkness. On day 1 and day 2, rats were exposed to a 12 hr fluorescent light,

from CT16 (11 P.M.) to CT4 (11 A.M.). After the light exposure, rats were transferred to constant darkness. The brain samples were collected during the Day0 or during the Day4 every 2h. Arrowheads indicate the sampling points of rats. ZT, Zeitgeber time; CT, Circadian time.

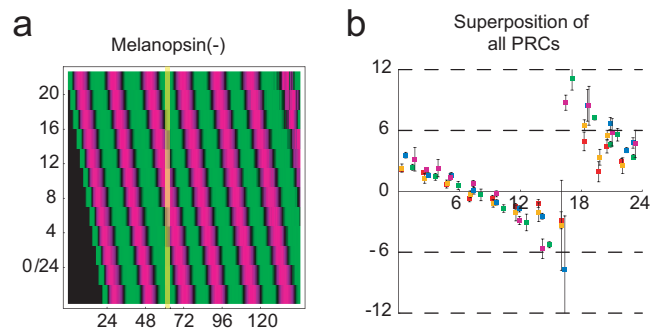


Figure S9 Effect of photo-perturbation on phase shift of melanopsin (-) cells. (a) High-throughput analysis of phase shifts of melanopsin (-) cells induced by 3h light pulses (yellow) of various timings. Magenta and green denote high and low normalized *PER2*-luciferase reporter activities.

(b) Superposition of all phase response curves (PRCs) of the *PER2*-luciferase reporter activities shown Fig.2. The phase shifts of melanopsin-positive cells are plotted against the timings of light pulses in circadian time (CT).

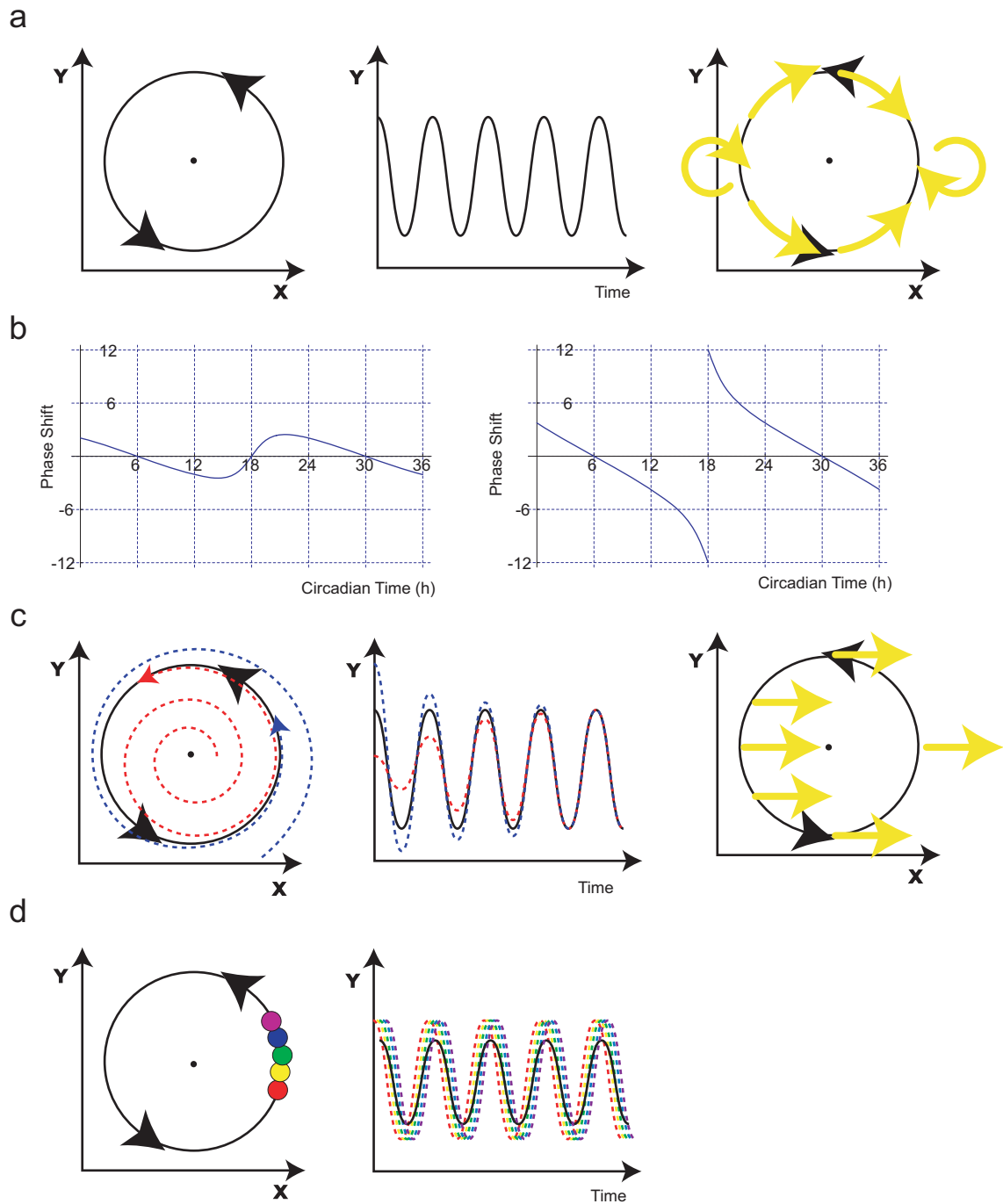


Figure S10 Schematic diagrams of the theoretical models for circadian clocks. **(a)** The simple clock model; its stable orbit and trajectory (a black line) shown in 2-dimensional phase space (left panel) and in 1-dimensional time course (middle panel). Possible perturbations to the simple clock oscillator are shown in yellow arrows (right panel). **(b)** Typical type 1 (left panel) and type 0 (right panel) phase response curves. **(c)** The simple limit-cycle model; its stable orbit (a black line) and trajectories after perturbations from the stable orbit (blue and red dashed lines) shown in 2-dimensional

phase space (left panel) and in 1-dimensional time course (middle panel). Possible perturbations to the limit-cycle oscillator are shown in yellow arrows (right panel). **(d)** The clockshop model; the common stable orbit (a black line) and individual states of multiple circadian oscillators (colored circles) shown in 2-dimensional phase space (left panel), and individual trajectories of multiple circadian oscillators (colored dashed lines) and their superposition (a black line), which is defined as the average of individual trajectories, shown in 1-dimensional time course (right panel).

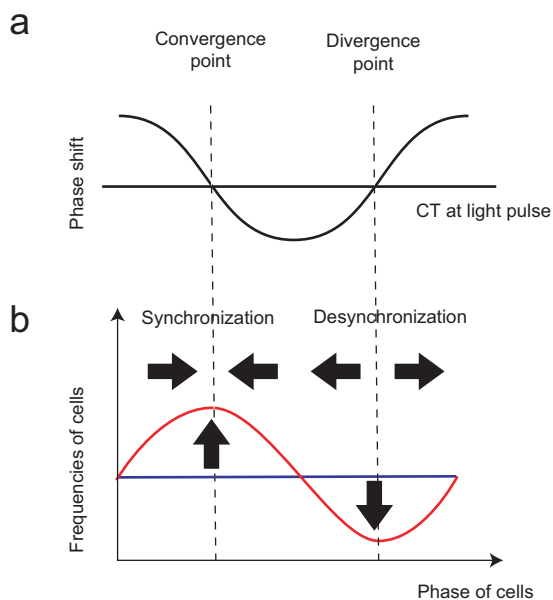


Figure S11 Schematic illustration of the recovery mechanism of amplitude induced by the second light pulse. **(a and b)** Schematic representation of single-cell-level PRC**(a)** and change in phase distribution induced by the second light pulse**(b)**. Blue curve represents the flat distribution of phase of cells induced by the first critical light-pulse. Red curve illustrates the

distribution of phase after the second light-pulse. By the second light pulse, the phase of cells near convergence point get synchronized, and those near divergence point desynchronized, resulting in the increase and decreases in frequencies of cell in the distribution around convergence and divergence point, respectively.

Number of figures	Number of cultures	Number of experiments	Remarks
1	n = 6	2	
S1	n = 6	4	
2, 3, S2	n = 2	1	0.5h light pulse
	n = 2	1	1.0h light pulse
	n = 2	3	3h light pulse
	n = 2	2	6h light pulse
	n = 2	2	12h light pulse
S3	n = 2	1	Light pulse at second day
	n = 2	3	Light pulse at third day
4	n = 1	3	Melanopsin-negative cell
	n = 1	3	Melanopsin-positive cell (Light pulse at timing of desynchronization)
	n = 1	1	Melanopsin-positive cell (Light pulse at timing of synchronization)

Table S1 The number of cultures used for a plot in each experiment, and the number of each experiment. “Number of cultures” represents the number of cultures used for a plot per an experiment. “Number of experiments” represents the number of each experiment that was independently performed. The corresponding experiment is indicated in the “Remarks”.

Movie Legends

Supplementary Movie 1 Single-cell bioluminescence imaging of melanopsin-negative cells exposed to a critical light pulse. Time-lapse image of melanopsin-negative cells exposed to a critical light pulse (yellow). Bioluminescence from cells is pseudo-colored.

Supplementary Movie 2 Single-cell bioluminescence imaging of melanopsin-positive cells exposed to a critical light pulse. Time-lapse image of melanopsin-positive cells exposed to a critical light pulse (yellow) capable of inducing multi-cell-level singularity behavior. Bioluminescence from cells is pseudo-colored.

Supplementary Movie 3. Single-cell bioluminescence imaging of melanopsin-positive cells exposed to a light pulse capable of increasing the averaged amplitude. Time-lapse image of melanopsin-positive cells exposed to a light pulse (yellow) capable of increasing the averaged amplitude of the cellular clocks. Bioluminescence from cells is pseudo-colored.

Supplementary Data

for

Melanopsin-dependent photo-perturbation reveals desynchronization underlying the singularity of mammalian circadian clocks

Hideki Ukai^{1*}, Tetsuya J. Kobayashi^{1,4*}, Mamoru Nagano⁵, Koh-hei Masumoto¹,
Mitsugu Sujino⁵, Takao Kondo⁶, Kazuhiro Yagita^{7,8}, Yasufumi Shigeyoshi⁵ and Hiroki
R. Ueda^{1,2,3}

¹*Laboratory for Systems Biology and ²Functional Genomics Unit, Center for
Developmental Biology, RIKEN, 2-2-3 Minatojima-minamimachi, Chuo-ku, Kobe,
Hyogo 650-0047, Japan.*

³*Department of Bioscience, Graduate School of Science, Osaka University, Toyonaka,
Osaka 560-0043, Japan.*

⁴*Research Fellow of Japan Society for the Promotion of Science.*

⁵*Department of Anatomy and Neurobiology, Kinki University School of Medicine, 377-2
Ohno-Hagashi, Osaka-Sayama, Osaka 589-8511, Japan*

⁶*Division of Biological Science, Graduate School of Science, Nagoya University and CREST & SORST, Japan Science and Technology Corporation, Furo-cho 1, Chikusa, Nagoya 464-8602, Japan.*

⁷*COE Unit of Circadian Systems, Division of Molecular Genetics, Department of Biological Sciences, Nagoya University Graduate School of Science, Furo-cho, Chikusa-ku, Nagoya, 464-8602, Japan.*

⁸*Department of Cell Biology and Neuroscience, Osaka University Graduate School of Medicine, 2-2 Yamadaoka, Suita, Osaka, 565-0871, Japan*

***These authors contributed equally to this work.**

Correspondence and requests for materials should be addressed to H.R.U. (e-mail: uedah-ky@umin.ac.jp).

SUPPLEMENTARY METHODS

Plasmid construction.

The pCMVTnT vector (Promega) was modified using the following method: Annealed complementary oligonucleotides (EcoRI-S.D./Kozak-Met-FLAG-I-SceI-XbaI) (Hokkaido System Science) containing EcoRI recognition sequence - Shine-Dalgarno sequence - Kozak sequence – Met codon – FLAG - *I-SceI* recognition sequence - XbaI recognition sequence were digested with EcoRI and XbaI and subcloned into EcoRI – XbaI site of pCMVTnT (hereafter referred to as plasmid A). Another annealed complementary oligonucleotide (XbaI-PI-PspI-stop-stop-NotI) containing XbaI recognition sequence - PI-PspI recognition sequence – tandem stop codon - NotI recognition sequence was next digested with XbaI and NotI and inserted into XbaI – NotI digested plasmid A (hereafter referred to as plasmid B). The region from the PstI recognition sequence to the NotI recognition sequence of plasmid B was amplified using PCR with forward primers (PstI-ICeuI-forward) containing the PstI and ICeuI recognition sequence and reverse primers (Sall-PI-SceI-reverse) containing the Sall and PI-SceI recognition sequence. PCR products were digested with PstI and Sall, and cloned into the PstI - Sall site of pCMVTnT (hereafter referred to as plasmid C).

Plasmid C was found to have a hairpin structure on the EcoRI recognition sequence in close proximity to the Kozak sequence, and this structure reduced transcription efficiency. In order to improve transcription efficiency, plasmid C was digested with EcoRI, blunt-ended with T4 DNA polymerase, and self-ligated. As a result, the hairpin structure was removed (hereafter referred to as plasmid D). pBC-KS(+) (Stratagene) plasmid was partially digested with PvuII, and a 2.9 kbp fragment containing replication origin and the *Chloramphenicol Acetyltransferase* gene was purified. Plasmid D was completely digested with BglIII and BamHI, and a 1.5 kbp fragment containing promoter-ORF cloning site was purified. The 1.5 kbp fragment from plasmid D were ligated into a 2.9 kbp fragment derived from pBC-KS(+). This resulted in the antibiotic resistance gene being converted from *β -Lactamase* to *Chloramphenicol Acetyltransferase*. The end product was named pMU2, and the useful ORF-cloning cassette in this vector was termed HU2 cassette.

The PCR product containing multiple cloning sites derived from pGL3-Basic (Promega) was amplified with primers (PvuI-MCS-forward and PstI-MCS-reverse), and digested by PvuI and PstI. The PvuI-PstI region of pMU2 containing the CMV-promoter was then replaced with the PCR product. The resulting vector was named pMU2-MCS. To drive the expression of melanopsin by the *GAPDH*-promoter, a

PCR product containing *GAPDH* promoter was amplified with primers (P(*GAPDH*)-MluI-forward and P(*GAPDH*)-BglIII-reverse), digested by MluI and BglIII, and then cloned into the MluI-BglIII region of pMU2-MCS. The resulting vector was named pMU2-P(*GAPDH*)-control.

Primers:

EcoRI-S.D./Kozak-Met-FLAG-I-SceI-XbaI:

5'-GAATTCGAAGGAGAGGCCACCATGGACTACAAGGATGACGATGACAAGA
ATTACCCTGTTATCCCTAATTCTAGA-3'

XbaI-PI-PspI-stop-stop-NotI:

5'-TCTAGATGGCAAACAGCTATTATGGGTATTATGGGTTAATGAGCGGCCGC-3'

PstI-ICeuI-forward:

5'-CTGCAGTAACTATAACGGTCCTAAGGTAGCGAAAGTTGGTCGTGAGGCAC
TG-3'

SalI-PI-SceI-reverse:

5'-GTCGACTGCCATTTTCATTACCTCTTTCTCCGCACCCGACATAGATTCATTAA
CCCATAATACCCATAATAGC-3'

PvuI-MCS-forward:

5'-CGATCGGGTACCGAGCTCTTACGCG-3'

PstI-MCS-reverse:

5'-CTGCAGAAGCTTACTTAGATCGCAG-3'

P(*GAPDH*)-MluI-forward:

5'-ACGCGTAATGAGGCGGGTCCAAAGAG-3'

P(*GAPDH*)-BglIII-reverse:

5'-AGATCTGCTTGCACACTTCGCACCAG-3'

Pharmacological assays.

Drugs used in the inhibition experiments were applied 1 hr before light pulse. U-73122

and BAPTA-AM were obtained from Sigma Aldrich and Dojindo, respectively.

Preprocessing of bioluminescence data. The bioluminescence from each sample was measured with multiple detectors. The data from individual detectors were normalized by the averaged intensity over time. The normalized data were then averaged over different detectors for the same sample at each time point to obtain the bioluminescence data for the sample. Data from impaired detectors were removed before averaging.

Baseline trends were detrended by the smoothing spline method as described previously¹. The same parameters¹ were used, except that in this case all time points were used for the detrending.

Quantification of multi-cell-level phase shift and amplitude change induced by light pulse.

To evaluate the phase and amplitude change purely induced by the light pulse, we selected four independent samples by removing two samples whose phases were insufficiently reset by the forskolin stimulation from the six samples prepared for each condition. The detrended data from each sample was normalized by the amplitude of the second peak. In Figure 1b, the average and standard deviation over four independent

samples were calculated at each time point. In order to calculate the phase shift and amplitude change shown in Figures 1c and Supplementary Figure S1, peaks from the normalized data were estimated by fitting the cubic polynomial to five neighboring time points, to obtain the timing and amplitude of the fourth peak, T_4 and A_4 , and the timing of the second peak, T_2 . The interval between the fourth and second peaks, $T_4 - T_2$, were used to calibrate the slight fluctuations of samples before the light pulse. The phase shift and amplitude change were obtained by comparing $T_4 - T_2$ and A_4 between samples with or without light-pulse exposure.

Data processing of high-throughput real-time reporter assays.

For the data in Figures 2, 3 and Supplementary Figures S2, S3, the average luciferase-reporter activities of different detectors for individual samples were calculated and then detrended as described above. To evaluate the phase and amplitude change purely induced by the light pulse, we removed samples whose phase was insufficiently reset by the forskolin stimulation from further data analysis.

Quantification of multi-cell-level phase shifts induced by light pulse in high-throughput real-time reporter assays.

First, the moving average of the absolute value of the detrended data was calculated.

The window size of the moving average was set to half of the period of the oscillation s estimated by autocorrelation from the detrended data, as described previously¹. The oscillatory component of the detrended data shown in Figures 2a, b and Supplementary Figures S2 and S3 a,b was calculated by dividing the data by the moving average data at each time point.

To obtain the phase shifts shown in Figure 2c and Supplementary Figure S3c, we calculated the differences between the peak timings of melanopsin-positive and -negative cells for individual peaks following light pulses. The average and standard deviation of phase shifts were calculated over individual peaks. The timings of light pulses and the phase shifts were then converted to circadian time (CT) by dividing them by the period of the corresponding melanopsin-negative cells. The time of the forskolin stimulation was set to CT0.

Notably, these multi-cell-level PRCs resemble light-type PRCs observed in mammals at the organism-level^{2,3} although there are some differences between phase shifts induced in cells and organism. First, phase shifts at the organism-level exhibit a dead zone, while phases shifts of cells exhibits no dead zone. Second, the averaged magnitude of cellular phase shifts is relatively larger than that of organismal phase shifts.

These properties observed at the organism-level might be attributed to a gating and/or coupling mechanism of multiple individual clock cells, both of which are known to exist in the organism. Thus, our cellular system will provide a synthetic-biological platform to test a hypothesis whether these organismal-level properties of phase shifts can be conferred by a gating and/or coupling mechanism.

Quantification of multi-cell-level amplitude changes induced by light pulse in high-throughput real-time reporter assays.

To extract the amplitude trends shown in Figure 3b, we first calculated the moving averages of the detrended data of melanopsin-positive and -negative cells as described above. The moving average data of the melanopsin-negative cells was fitted by an exponential function. The moving average data of the melanopsin-positive cells was then divided by the exponential function of the corresponding melanopsin-negative cells. Finally, the data was fitted by a cubic spline function to obtain the long-term trend in the amplitude change shown in Figure 3b. Each amplitude response in Figure 3c and Supplementary Figure S3d was calculated by averaging the amplitude change over two days after the light pulse. The timings of light pulse were converted to CT as described above.

Data processing for real-time single-cell bioluminescence imaging.

Supplementary Fig. S4 shows nine representative single-cell-level bioluminescence of melanopsin negative and positive cells to which temporal moving average with 1-hour window size was applied to the data for 10 iterations to remove local peaks attributable to measurement noise and anomalous behavior of individual cells. To obtain the data in Figure 4c and Supplementary Figure S5b, the bioluminescence data of each cell was normalized so that its maximum and minimum intensities respectively became one and zero. The data used in Figure 4d, e and Supplementary Figure S5b was obtained by applying the detrended baseline and subsequent normalization to each cell's original data. The processed bioluminescence data were then sorted by their peak timings. Before determining the peak timing, temporal moving average with 1-hour window size was applied to the data for 10 iterations. The peak timings were then determined by fitting cubic polynomial to the five neighboring time points as described above. To sort the data of individual cells by their peak timings, we first calculated the first four peaks of the average bioluminescence of all cells. This was then followed by collecting the closest peak of each cell to the corresponding peak of the averaged data.

To quantify the single-cell-level amplitude, we calculated average and standard deviation of amplitude of 2nd, 3rd, 4th, and 5th peaks of the single-cell-level bioluminescence data (Supplementary Fig. S5 a). The figure demonstrates that the critical light pulse induces no significant change in the average amplitude, indicating that the amplitude decrease or increase in multi-cell-level can be attributed to desynchronization and synchronization of cells.

To quantify the desynchronization and synchronization observed in Figure 4c-d and Supplementary Figure S5b, we calculated cumulative plots of phase where the sorted phases of individual cells are cumulatively plotted against the percentage of cells (Supplementary Figure S5c). The phases of cells are normalized so that their median value is zero.

Data processing of *in situ* hybridization images.

In order to quantify the spatio-temporal expression pattern shown in Figure 5a, the number of *Per1* and *Per2* mRNA-positive cells was counted twice, separately in dorsomedial (DM) and ventrolateral (VL) regions of the rat SCN, in slices with clear separation of these two sub-regions (three sections per animal). A blinded observer made two separate counts of the number of positive cells within DM region, VL region

and the entire SCN⁴. Cells were counted only when the cytoplasm was clearly labelled against the background. As a result, there was good agreement in the numbers between the two rounds of counting. The average numbers of positive cells per single suprachiasmatic nucleus at each time point were plotted. The DM region was distinguished from the VL region by using morphological criteria described previously⁵.

While the manual counting of positive cells is a generally adopted procedure to quantify the spatio-temporal expression from *in situ* hybridization images, it is difficult to obtain the information on more local expression patterns within the entire SCN by manual counting. To complement manual counting, we developed a computer program that can automatically analyze the *in situ* hybridization image of SCN slices (Supplementary Figure S6). We first converted the original *in situ* hybridization images to grayscale by averaging red, green and blue intensities of each pixel. To reduce the local noise in images, we applied spatial moving average filter whose window size was 20×20 pixels, and then converted the image from 700×700 to 220×220 pixels. Each grayscale image was normalized so that the average intensity of right top corner (*Per1*) or right and bottom sides (*Per2*) of the image was 1000. These areas were used as reference because the positive cells were rarely observed in these areas. The time series of each pixel was approximated by interpolating them with a cubic

spline curve. Since we obtained three slices for each SCN sample and we conducted *in situ* hybridization of two independent samples for each time point, we used six intensity data for each time point to obtain the cubic spline fitting curve. The spline fitting curves were then normalized so that the maximum and minimum intensities of all spline curves become 0 and 1, respectively (Since the pixels of positive cells, i.e. dark pixels, have lower intensity in the *in situ* hybridization images, the pixels of positive cells are converted to higher value by this normalization). To obtain Supplementary Figure S6, we finally sorted the time series by their mean values so that time series of a pixel with a higher mean value has a lower index. As is shown in Supplementary Figure S6, the expression timings of clock genes in the control experiment were synchronized around CT4~8 for *Per1* and CT8~12 for *Per2* within the entire SCN (Supplementary Figure S6, upper panels) whereas the expression timings of both clock genes become spatially desynchronized after the critical light pulses (Supplementary Figure S6, lower panels). Similar diversification of expression timings are also evident for *Per1* (Supplementary Figure S6, left panels), indicating that the states of circadian clocks were spatially desynchronized in the entire SCN after the critical light pulses. This spatial desynchronization in the SCN was reproducibly detected in our repeated experiments,

indicating that the critical light pulses can robustly induce desynchronization of the SCN.

SUPPLEMENTARY RESULTS and DISCUSSION

The development of clock models.

Various theoretical models of circadian clocks have been developed in the last half century, from fairly simple ones to more sophisticated models to accommodate newly-discovered dynamical properties of circadian clocks.

The simplest of these is the “simple clock” model. The possible states of a simple clock model are located on a circle in a state space (Supplementary Fig. S10a online, left panel), implying that its amplitude is constant (Supplementary Fig. S10a online, middle panel) and that its dynamics are characterized only by its phase. Since its state is restricted to the circle, external perturbation imposed to the clock simply shifts its phase either forward, backward or unchanged (Supplementary Fig. S10a online, right panel). Mathematical analysis of the simple clock model easily demonstrates that the simple clock model only shows weak (type 1) phase response (Supplementary Fig. S10b online, left panel) to any external perturbations, and can exhibit neither the strong (type 0) phase response (Supplementary Fig. S10b online, right panel) nor the singularity behavior observed in organisms. Since most organisms exhibit both weak (type 1) and strong (type 0) phase response as well as singularity behaviors, the simple clock model has been excluded as a plausible explanatory model for circadian clocks.

The simple limit-cycle model was previously proposed to explain the strong (type 0) phase response and singularity behaviors. The simple limit-cycle model has a strongly attractive circular orbit and a unstable fixed point in a state space. Because of an attractive circular orbit, the simple limit-cycle model behaves like a simple clock model without external perturbation (Supplementary Fig. S10c online). In contrast to the restricted state within the orbit in the simple clock model, external perturbation can transiently bring the state of circadian oscillator outside the orbit in the simple limit-cycle model (Supplementary Fig. S10c online, right panel), and hence change the amplitude of circadian oscillation (Supplementary Fig. S10c online, middle panel) although it restabilizes quickly to the original attractive orbit (Supplementary Fig. S10c online, left panel). Based on the existence of this attractive orbit, the simple limit-cycle model is proved to accompany an unstable fixed point within its attractive orbit. Both strong (type 0) and weak (type 1) phase response, as well as singularity behavior, can be explained in the simple limit-cycle model based on the existence of this unstable fixed point. For example, singularity behavior of circadian clocks is explained in the simple limit-cycle model as the stopping of circadian oscillator at the unstable fixed point.

Despite its ability to explain weak (type 1) and strong (type 0) phase responses and singularity behaviors, however, the plausibility of the simple limit-cycle model was

questioned by Arthur T. Winfree in 1970s. In order to investigate how fast a circadian oscillator was recovered to its attractive orbit after various perturbations, Arthur T. Winfree and others conducted extensive two-pulse experiments^{6,7} and unexpectedly found the “unlocklike” behavior of circadian clocks where a circadian clock seemed to oscillate stably at a original frequency with a lower amplitude for a long time after particular perturbations, which apparently argued against the simple limit-cycle model. To accommodate this “unlocklike” behavior of circadian clocks, he proposed the “clockshop” hypothesis that an organism-level circadian clock consists of multiple circadian oscillators with substantial fluctuations (Supplementary Fig. S10d online, left panel), and that superposition of multiple circadian oscillators defines the output of the organism-level circadian clock (Supplementary Fig. S10d online, right panel). He also predicted that desynchronization of multiple circadian oscillators would underlie the observed “unlocklike” behavior (multi-cell-level amplitude decrease) of circadian clocks, although direct experimental verification of this prediction was impossible at that time due to the lack of technology to observe circadian rhythmicity at the single-cell-level.

Prediction of the underlying mechanism for the multi-cell-level singularity behavior from multi-cell-level data.

The underlying mechanism of the multi-cell-level singularity behavior in our system can be predicted from the multi-cell-level dynamical properties of cellular clocks represented in the obtained PRCs and ARCs (Fig. 2c and 3c). We first noticed that the timing of the minima in ARCs (or timing of singularity behaviors) closely match with those of delay-to-advance transition in PRCs (CT~17, near subjective midnight), and then discovered that this strong correlation between ARCs and PRCs can be consistently explained by the second mechanism (desynchronization of individual clocks). Suppose that the phases of multiple cellular clocks are distributed around CT~17, and that the single-cell-level PRC is close to the experimentally observed multi-cell-level PRC. In this scenario, delayed cells with a phase less than CT~17 receive a light pulse to delay their phase and as a result are driven further from CT~17, while the advanced cells with a phase of more than CT~17 receive the light pulse that advances their phase, moving them further from CT~17 as well. This suggests that a light pulse applied around CT~17 diversifies the phase of cellular clocks to decrease the averaged amplitude of cellular clocks, and hence can drive cellular clocks into the multi-cell-level singularity behavior in severe cases.

In addition, we also noticed that the timings of the maxima in ARCs closely match those of advance-to-delay transition in PRCs (CT~6, subjective noon), and realized that this correlation can be also explained by the same mechanism. Suppose that phases of multiple cellular clocks are distributed around CT~6, the delayed cells with a phase less than CT~6 receive a light pulse to advance their phase and then return to CT~6, while the advanced cells with a phase of more than CT~6 receive the light pulse to delay their phase and also come back to CT~6. This suggests that a light pulse around CT~6 converges the phase of cellular clocks to increase the averaged amplitude of cellular clocks. Since the increase of the averaged amplitude cannot be explained by the arrhythmicity of individual clocks without additional assumptions, we can predict that the desynchronization of individual clocks underlies the singularity behavior.

The desynchronization of individual clocks predicted above can also explain the recovery of multi-cell-level oscillation by the second light pulse observed in Figure 4a. As already mentioned, the first critical light pulse desynchronizes the phase of cellular oscillators, resulting in the uniform distribution of the phase schematically described with blue line in Supplementary Figure S11. When the second pulse is applied to cells, cells whose phase are close to the “phase convergence” point of PRC become synchronized, while cells whose phase are close to the “phase divergence” point

become desynchronized. Because of these synchronization and desynchronization processes, the population at the “phase convergence” point becomes increased while the population at “phase divergence” point becomes decreased. As a result, the distribution of the phase will change from uniform distribution (blue line) to ununiform distribution peaked around “phase convergent” point (red line). This ununiform distribution results in the recovery of multi-cell-level oscillations as observed in our experiment.

While this prediction is not always necessary in this study due to direct verification by single-cell-level measurement, the analysis described here is still worth noting because we can apply this to inspect underlying mechanism of singularity behaviour in other organism from their multi-cell-level data.

Synchronization underlying multi-cell-level amplitude increase.

To verify not only desynchronization underlying singularity behavior but also synchronization underlying amplitude increase predicted above, melanopsin-positive cells were exposed to a light pulse capable of increasing the averaged amplitude of the cellular clocks (Supplementary Figure S5b, Supplementary Figure S5c right panel, and Supplementary Movie 3 online). As expected, we observed that the slopes of the third

and second peaks were almost identical in melanopsin-positive cells (Supplementary Figure S5c right panel) while the slope of third peak is larger than that of the second peak in melanopsin-negative cells. This result indicates that the light pulse applied to melanopsin-positive cells induces synchronization of phases, which negates the diversification of phases over time. We also verified that the light pulse did not induce detectable increase in single-cell-level amplitude (Supplementary Figure S5a online). Thus, the same single-cell-level mechanism (synchrony control of cellular clocks by light pulse) can consistently explain the multi-cell-level amplitude increase induced by a light pulse around CT~6.

Theoretical model for the multi-cell-level phase shift and amplitude change.

In an attempt to quantitatively reproduce the multi-cell-level phase shift and amplitude change, we constructed a mathematical model of multiple cellular clocks. To model single-cell behavior, we adopted the simple limit cycle model that features a strongly attractive stationary orbit⁷. The strong attractive stationary orbit of our circadian oscillator in a single cell is supported by the no substantial difference between the average amplitudes of the oscillators before and after the light pulse (Supplementary Fig. S5a). While this assumption is not generally valid, in our system it is experimentally

verified as we experimentally observed that most of cells quickly recovered their oscillation within one cycle after the light pulse. Given this assumption, the oscillation of individual cells can be characterized by its phase, θ , defined on a unit circle. As we use approximately 1×10^6 cells to measure the multi-cell-level response for each experimental condition, we can also assume that the number of cells in a population is large enough so that the percentage of cells whose phase is θ at time t can be represented by a probability density function, $P(t, \theta)$. For simplicity of analysis, $P(t, \theta)$ is assumed to satisfy $P(t, \theta) = P(t + \Delta t, \theta + \omega \Delta t)$ without external perturbation. This assumption means that the distribution of the phase moves with period $1/\omega$ without changing shape, and that the change of the distribution is induced only by the external perturbation. This modeling was approximately varied for analyzing our data, since the phase shift and amplitude change induced by other perturbation or intracellular noise than light pulse were computationally removed by comparing melanopsin-positive and -negative cells in our experimental data. A more detailed model to ensure this simplification will be described elsewhere (T.J.K. *et al* in preparation).

After the application of the light pulse at time t_1 , individual cells are assumed to change their phases according to a single-cell-level phase response curve (PRC). As

we have so far been unable to obtain the single-cell-level PRC experimentally, we assume that the PRC can be described as

$$PRC(\theta, \alpha) = \arg(\exp[2\pi i\theta] + i\alpha) / 2\pi - \theta, \quad (S1)$$

where i represents the imaginary unit^{7,8}. The parameter α describes the intensity of the phase shift (i.e. a larger α represents the longer or stronger perturbation of cellular clocks). With this single-cell-level PRC, the single-cell-level phase transition curve (PTC) can be defined as $PTC(\theta, \alpha) = \theta + PRC(\theta, \alpha)$. The parameter α abstractly represents the intensity of the perturbation, and the perturbation with higher strength or longer duration is therefore assumed to be represented with higher α in our model. The PRC has qualitatively different properties depending on the value of α . When a perturbation is weak, specifically $\alpha < 1$, then PRC displays relatively small phase shifts and has a continuous transition from delays to advances at the phase divergence point. The phase divergence point in eqn. S1 is $\theta = 3/4$, which corresponds to circadian time (CT) 18 (subjective midnight), when we define CT0 as $\theta = 0$. In contrast, when a perturbation is strong, specifically $\alpha > 1$, then PRC displays large phase shifts and has a discontinuous transition from delays to advances at the phase divergence point. The former and the latter are called type-1 and type-0 PRCs, respectively, as the average slopes of the corresponding PTCs are respectively 1 and 0. The simple limit cycle

model predicts that the perturbation with the strength $\alpha = 1$ applied at the phase divergence point is the critical perturbation that can induce the singularity behavior of a limit cycle as $(\alpha, \theta) = (1, 3/4)$ is the only point at which $PRC(\theta, \alpha)$ cannot be defined.

We assume that $\bar{P}(t, \theta)$ is the probability density function of the phase of oscillators after the light pulse. As the oscillators typically show transient dynamics after the light pulse, the actual $\bar{P}(t, \theta)$ depends on the detail of dynamics of the individual oscillator. Rather than model such complex transient dynamics, we define $\bar{P}(t, \theta)$ as the extrapolation of the phase distribution of oscillators after the transient dynamics. The validity of this definition is experimentally supported by our observation that the oscillations of individual cells were recovered within one cycle after the light pulse. Furthermore, in our data analysis, the multi-cell-level phase shift and amplitude change were calculated as the averages of several cycles after the light pulse, which will attenuate the effect of transient dynamics. We also assume $\bar{P}(t, \theta) = \bar{P}(t + \Delta t, \theta + \omega\Delta t)$. With these definitions of the PTC and $\bar{P}(t, \theta)$, we have the relationship between the distributions before and after the light pulse as follows:

$$\bar{P}(t_1, \bar{\theta})d\bar{\theta} = P(t_1, \theta)d\theta, \quad \bar{\theta} = PTC(\theta),$$

where $\bar{\theta}$ represents the phase after the light pulse.

In our experiment, the multi-cell-level phase shift and amplitude change were calculated from total luciferase reporter activities from the population of cells. To model single-cell-level luciferase reporter activity, we assume that the activity of the individual cell is represented as $F(t) = F(\theta(t))$ where $F(\theta)$ is a periodic function on the unit circle. For simplicity of analysis, we use $F(\theta) = \sin(2\pi\theta)$. In this case the multi-cell-level activity of the population before the light pulse, $A(t)$, can be described as

$$A(t) = \int F(\theta)P(t, \theta)d\theta = \int \sin(2\pi\theta)P(t, \theta)d\theta. \quad (\text{S2})$$

Similarly, the average activity after light pulse, $\bar{A}(t)$, can be described as

$$\bar{A}(t) = \int F(\bar{\theta})\bar{P}(t, \bar{\theta})d\bar{\theta} \quad (\text{S3})$$

To calculate $A(t)$ and $\bar{A}(t)$, we require detailed information on $P(t, \theta)$. For modeling $P(t, \theta)$, we used a Gaussian distribution defined on a unit circle:

$$P(t, \theta) = \sum_{k \in \mathbb{Z}} \frac{1}{\sqrt{2\pi\sigma^2}} \exp\left(\frac{-(\theta - \omega t - \theta_0 + k)^2}{2\sigma^2}\right),$$

where θ_0 and σ describe the average phase of cells at $t = 0$ and the variation of phases, respectively.

Simulation of the multi-cell-level phase shift and amplitude change.

To obtain the multi-cell-level phase shift and amplitude change, we numerically calculated $A(t)$ and $\bar{A}(t)$ with eqns. S2 and S3 for various σ , α , and θ_0 , with ω was set to 1 without losing generality. The multi-cell-level phases shift and amplitude change were calculated from the peaks of $A(t)$ and $\bar{A}(t)$. We then obtained the multi-cell-level PRCs and ARCs for each parameter set of σ and α by plotting the phase shifts and amplitude changes against θ_0 . The timings of light pulses in all PRCs and ARCs shown in Figure 2c and 3c are converted from the unit circle to CT.

The best fitted simulation data in Figures 2c and 3c were searched by measuring difference between the experimental data and simulated data for various parameter sets of σ and α . We found that the simulated data whose $\sigma = 0.24$ can reproduce the experimental data qualitatively. This value was consistent with the estimated value of the phase distribution from the single-cell measurement. This estimation was conducted by comparing the standard deviation of the timings of the second peak collected from the single-cell experimental data and that of the Gaussian distribution with fixed σ defined on a unit circle. The parameter values of α were 0.35, 0.4, 0.65, 0.7, and 0.95 for 0.5, 1, 3, 6, and 12-hour light duration data, respectively. The identified α values for different light pulses are consistent with the durations of light pulses. As shown in Figures 2c and 3c, the types of the PRCs, and the

maximum and minimum values of ARCs as well as their shapes were qualitatively reproduced by the simulation. This remarkable agreement between simulation and experiment suggests that possible intercellular variations of melanopsin expression due to transient transfection make a minor contribution, if any, to the multi-cell-level phenotype, since intercellular variations of melanopsin expression are not included in our simulation model. In addition, we also observed more than 2-fold amplitude change due to the synchronization of cellular clocks, which would hardly be observed if the variation of melanopsin was the dominant source of intracellular noise inducing the desynchronization. The simulation furthermore suggests that the multi-cell-level singularity behavior and the transition of the types of PRC from 1 to 0 occurs simultaneously similarly to the simple limit cycle model, as described above. This result indicates that the multi-cell-level singularity behavior is barely induced if perturbations such as drug administration and temperature change are too strong to always induce multi-cell-level type-0 phase response, or are too weak to always induce multi-cell-level type-1 phase response.

Theory demonstrates that desynchronization is a plausible mechanism of observability of singularity behavior.

The simple limit-cycle model predicts that the singularity behavior can be induced merely by the infinitesimal range of perturbation strength and timing, which is hard to realize by experiment, standing in sharp contrast with the reproducible and prevalent observations of singularity behaviors in various organisms. To test how the observability of singularity can be explained by our model, we calculated the amplitude change as a function of timing and strength of light pulse for various values of σ . As shown in Supplementary Figure S7, the parameter range in which substantial amplitude decrease can be observed (green regions in Supplementary Figure S7) expand as the phase variation of a population of cells before light pulse increases. Hence, if there are substantial fluctuations in the state of individual cellular clocks, then the multi-cell-level singularity behavior will be stably and robustly induced by the experimentally achievable range of perturbation strength and timing, which has been shown in our *in vitro* system (**Fig. 4**). Since recent single-cell-level measurement of individual cellular clocks in the SCN revealed substantial fluctuations in the states of central clocks^{9,10}, our model predicts that desynchronization of cellular clocks in the SCN can be stably induced by the critical light pulses. This prediction is quite consistent with our robust

observations that the desynchronization actually underlies the multi-cell-level amplitude decrease in the SCN after the critical light pulses that can also probabilistically induce temporal amplitude decrease of locomotor activity. Furthermore, recent single-cell-level measurement have revealed substantial fluctuations in the state of cellular clocks in the peripheral or in other organism¹¹⁻¹³, and it is reasonable to suppose that substantial fluctuations exists in cellular clocks in general, probably due to the intracellular noise ubiquitous in living systems¹⁴⁻¹⁶. Given the substantial fluctuations in cellular clocks , our model can further explain why multi-cell-level singularity behaviors have been experimentally observed in various organisms. On the basis of these results and considerations, we propose desynchronization as a plausible mechanism underlying the observable singularity behaviors of circadian clocks.

As pointed out in the body, however, we cannot completely exclude the simple limit cycle model because the ability of stopping the individual oscillators depends on the amplitude of the stable limit cycle, the magnitude of the basin of attraction bounding the phase-less set and so on. For example, extensions of the simple limit-cycle model such as the limit-cycle model with stable fixed point^{17,18} or two-step mechanism¹⁹ have been proposed to explain the prevalent singularity behaviors. While the extended model can explain the prevalent experimental observation of singularity behaviors, further

modifications is required to accommodate the observed “unclocklike” behavior of circadian clock.

Since a model can be extended to incorporate unexplained observations, validation of the generality of the proposed desynchronization mechanism will require the direct verification of underlying mechanism of singularity behaviors in other circadian systems such as *Neurospora* clock cells, where singularity behaviors have been beautifully observed *in vivo*¹⁹, and zebrafish clock cells, which can respond to a light pulse and can be measured *in vitro* at the single-cell level^{13,20}. In any case, the direct verification by single-cell measurement plays critical role for the validation.

Limitations of the theoretical model.

While our model qualitatively reproduces the experimental data, it has some limitations due to its simplicity. First, as α is an abstract parameter representing the intensity of the perturbation, α is generally a complicated nonlinear function of the light strength and duration. We cannot therefore discuss the quantitative relationship between the values of α in our simulation and the corresponding durations of light pulses. From a theoretical viewpoint, however, α is expected to monotonously depend on the

strength or duration of light pulse. This qualitative relationship between α and light duration was reproduced in our results (Figure 2c and 3c).

Second, in our simulation the positions of the minima of the ARCs were not quantitatively reproduced. This deviation can be attributed to the simplification of our model, with one possibility being, for example, that the real single-cell PRC has its divergence point at CT~16 or CT~17 while the divergence point in our model locates at CT18. This deviation can be corrected by using a more complicated equation for describing the single-cell-level PRC.

Third, our model does not include intercellular interactions, which play a crucial role in circadian oscillation of some organisms. The influence of incorporation of intercellular interactions strongly depends on the intrinsic dynamical property of individual circadian oscillator and type of coupling. When phase shift induced by light pulse is weakly influenced by the coupling, our model can be naturally extended to interacting cells as the phase shifts and amplitude changes are determined in our model depending on the mean phase and phase variation of a population of cells at the moment of the light pulse. Incorporation of the intercellular interaction to our model will then explain additional dynamics of cells before and after the light pulse. For example, it is expected that the incorporation will be able to explain the recovery of multi-cell-level

oscillation by the re-establishment of the synchronized state from the desynchronized state induced by the critical light pulse. The delay until recovery and the multi-cell-level phase after the recovery can also be explained by the extended model (T.J.K. *et al* in preparation). If the mutual interaction of coupling and light-induced perturbation is not weak, then we need to use more detailed model which can reproduce the dynamics of a circadian oscillator in a single cell observed experimentally. However, we lack experimentally observed quantitative data sufficient to model such detailed dynamics. Further advance in experimental measurement *in vivo* and synthetic implementation of circadian oscillation will enable us to construct the model that can handle these problems, and other properties of circadian oscillator such as the desynchronization of SCN neurons induced by constant light condition^{21,22}.

Finally, the existence of peripheral clocks and nonlinear amplification of input and output of core clocks may complicate the light response of the locomotor rhythmicity such as the probabilistic observation of temporal amplitude decrease in locomotor activity shown in Figure 5c. Since several brain regions express clock genes and these peripheral clock tissues can sustain oscillations for a couple of days without any signal from SCN²³⁻²⁶, the multi-cell-level amplitude decrease in the SCN might be transiently compensated by output peripheral clock region(s) more directly controlling

locomotor activities. Alternatively, the decreased multi-cell-level amplitude in the SCN might be amplified by nonlinear signal transduction(s). We also cannot completely exclude other possibilities, such as that the SCN region responsible and sufficient for locomotor activity control is restricted, with the small portion of SCN that is less than the experimentally detectable size in our pixel-level (several cells at most) image analysis. In either of the cases listed here, further modifications of our model will be required, for example, by introducing an intercellular network structure between central and peripheral clocks or signal transduction pathways downstream of SCN. To collect sufficient information for these modifications, further technological development enabling real-time quantitative perturbation and single-cell-level measurement simultaneously in living organisms will be needed.

While some of quantitative and qualitative deviations from the experimental data may be explicitly described using a more complicated and tangled mathematical model, we adopted the simplest model to avoid obscuring the conceptual essence by unnecessary complexity. Because of this simplicity, our model can be used to investigate desynchronization underlying various multi-cell biological oscillators such as cardiac and respiratory oscillation²⁷.

References

1. Sato, T.K. et al. Feedback repression is required for mammalian circadian clock function. *Nat Genet* **38**, 312-9 (2006).
2. Johnson, C.H. Forty years of PRCs--what have we learned? *Chronobiol Int* **16**, 711-43 (1999).
3. Dunlap, J.C., Loros, J.J. & DeCoursey, P.J. (eds.). *Chronobiology: Biological Timekeeping*, (Sinauer Associates, Inc., Sunderland, Massachusetts, U.S.A, 2004).
4. Nagano, M. et al. An abrupt shift in the day/night cycle causes desynchrony in the mammalian circadian center. *J Neurosci* **23**, 6141-51 (2003).
5. Van den Pol, A.N. The hypothalamic suprachiasmatic nucleus of rat: intrinsic anatomy. *J Comp Neurol* **191**, 661-702 (1980).
6. Winfree, A.T. Unclocklike behaviour of biological clocks. *Nature* **253**, 315-9 (1975).
7. Winfree, A.T. *The Geometry of Biological Time*, (Springer-Verlag, New York, 1980).
8. Johnson, C.H., Elliott, J.A. & Foster, R. Entrainment of circadian programs. *Chronobiol Int* **20**, 741-74 (2003).
9. Maywood, E.S. et al. Synchronization and maintenance of timekeeping in suprachiasmatic circadian clock cells by neuropeptidergic signaling. *Curr Biol* **16**, 599-605 (2006).
10. Yamaguchi, S. et al. Synchronization of cellular clocks in the suprachiasmatic nucleus. *Science* **302**, 1408-12 (2003).

11. Welsh, D.K., Yoo, S.H., Liu, A.C., Takahashi, J.S. & Kay, S.A. Bioluminescence imaging of individual fibroblasts reveals persistent, independently phased circadian rhythms of clock gene expression. *Curr Biol* **14**, 2289-95 (2004).
12. Nagoshi, E. et al. Circadian gene expression in individual fibroblasts: cell-autonomous and self-sustained oscillators pass time to daughter cells. *Cell* **119**, 693-705 (2004).
13. Carr, A.J. & Whitmore, D. Imaging of single light-responsive clock cells reveals fluctuating free-running periods. *Nat Cell Biol* **7**, 319-21 (2005).
14. Rao, C.V., Wolf, D.M. & Arkin, A.P. Control, exploitation and tolerance of intracellular noise. *Nature* **420**, 231-7 (2002).
15. Kaern, M., Elston, T.C., Blake, W.J. & Collins, J.J. Stochasticity in gene expression: from theories to phenotypes. *Nat Rev Genet* **6**, 451-64 (2005).
16. Raser, J.M. & O'Shea, E.K. Noise in gene expression: origins, consequences, and control. *Science* **309**, 2010-3 (2005).
17. Leloup, J.C., Gonze, D. & Goldbeter, A. Limit cycle models for circadian rhythms based on transcriptional regulation in *Drosophila* and *Neurospora*. *J Biol Rhythms* **14**, 433-48 (1999).
18. Leloup, J.C. & Goldbeter, A. A molecular explanation for the long-term suppression of circadian rhythms by a single light pulse. *Am J Physiol Regul Integr Comp Physiol* **280**, R1206-12 (2001).
19. Huang, G., Wang, L. & Liu, Y. Molecular mechanism of suppression of circadian rhythms by a critical stimulus. *Embo J* (2006).
20. Whitmore, D., Foulkes, N.S. & Sassone-Corsi, P. Light acts directly on organs and cells in culture to set the vertebrate circadian clock. *Nature* **404**, 87-91 (2000).

21. Granados-Fuentes, D., Prolo, L.M., Abraham, U. & Herzog, E.D. The suprachiasmatic nucleus entrains, but does not sustain, circadian rhythmicity in the olfactory bulb. *J Neurosci* **24**, 615-9 (2004).
22. Ohta, H., Yamazaki, S. & McMahon, D.G. Constant light desynchronizes mammalian clock neurons. *Nat Neurosci* **8**, 267-9 (2005).
23. Yamazaki, S. et al. Resetting central and peripheral circadian oscillators in transgenic rats. *Science* **288**, 682-5 (2000).
24. Yamaguchi, S. et al. The 5' upstream region of mPer1 gene contains two promoters and is responsible for circadian oscillation. *Curr Biol* **10**, 873-6 (2000).
25. Wilsbacher, L.D. et al. Photic and circadian expression of luciferase in mPeriod1-luc transgenic mice in vivo. *Proc Natl Acad Sci U S A* **99**, 489-94 (2002).
26. Yoo, S.H. et al. A noncanonical E-box enhancer drives mouse Period2 circadian oscillations in vivo. *Proc Natl Acad Sci U S A* **102**, 2608-13 (2005).
27. Forger, D.B. & Paydarfar, D. Starting, stopping, and resetting biological oscillators: in search of optimum perturbations. *J Theor Biol* **230**, 521-32 (2004).